



TECHNISCHE  
UNIVERSITÄT  
WIEN

Vienna University of Technology

DIPLOMARBEIT

# An 8-channel Receive-Only Radio Frequency Coil Array for Magnetic Resonance Microscopy at 7 Tesla

Ausgeführt an der Fakultät für Physik  
der Technischen Universität Wien

unter der Anleitung von

***Univ. Prof. Dipl. -Ing. Dr. techn. Gerald Badurek***

und

***Ass.-Prof. Dr. Elmar Laistler***

Medizinische Universität Wien

Zentrum für Medizinische Physik und Biomedizinische Technik

Abteilung MR Physik

durch

**Seyed Ehsan HOSSEINI**

Sonnenallee 49/6, 1220 Wien

Wien, am 1.8.2017

Unterschrift



# Erklärung zur Verfassung der Arbeit

Seyed Ehsan Hosseini

Sonnenallee 49/6, 1220 Wien

Hiermit erkläre ich, dass ich diese Arbeit selbständig verfasst habe, dass ich die verwendeten Quellen und Hilfsmittel vollständig angegeben habe und dass ich die Stellen der Arbeit – einschließlich Tabellen, Karten und Abbildungen –, die anderen Werken oder dem Internet im Wortlaut oder dem Sinn nach entnommen sind, auf jeden Fall unter Angabe der Quelle als Entlehnung kenntlich gemacht habe.

Wien, 01. Aug. 2017

---

Seyed Ehsan Hosseini



# Acknowledgements

I would first like to thank my thesis supervisor Dr. Elmar Laistler and my advisor Dr. Roberta Frass-Kriegl for the continuous support of my master study, for their patience, and motivations. I would also like to give special thanks to Prof. Andreas Berg, who invited me to the MR Center of Excellence and connected me to the RF group. I will never forget his scientific supports, as well as his attentions for introducing the micro imaging system to me.

I thank my supervisor Prof. Gerald Badurek, in the Department of Physics, for his useful lectures in MR, his guidelines, and assessment of this work. I take this opportunity to express gratitude to Dr. Karin Poljanc for her supports and efforts which resulted in my collaboration with the MR Division at Medical University of Vienna.

I appreciate Prof. Ewald Moser, Dean of the MR Division, for the continuous encouragement. Thanks also go to all my colleagues in RF lab for their helps, whenever I ran into a trouble spot or had a question.

Finally, I must express my gratitude to my mother, my partner and my family for providing me with unfailing support.

I acknowledge financial support from Mayor of Vienna (Hochschuljubiläumsfonds (HSJ) der Stadt Wien H-1208/2003, "MR-based dosimetry of High-LET radiation" (3D) proton and neutron dosimetry“) and the Austrian/French FWF/ANR Programme Blanc grant, Nr. I1371-B24, “FLEXAR7”.

*“Thank you again for giving me the opportunity to do this wonderful project.”*



# Table of Contents

Acknowledgements .....	5
Abstract .....	11
1 Introduction .....	13
2 Basic Principles .....	15
2.1 MRI Physics .....	15
2.2 High Field MRI .....	19
2.3 MR Microscopy .....	20
2.4 Radio Frequency Coils .....	20
2.4.1 General aspects .....	20
2.4.2 Tuning and matching .....	22
2.4.3 Transmission decoupling .....	24
2.4.3.1 Passive decoupling .....	25
2.4.3.2 Active decoupling .....	26
2.4.4 Coil arrays .....	27
2.4.4.1 Mutual decoupling .....	27
2.4.4.1.1 Overlap decoupling .....	28
2.4.4.1.2 Capacitive and inductive decoupling .....	28
2.4.4.1.3 Preamplifier decoupling .....	29
2.4.4.2 Parallel imaging .....	30
2.4.5 Sensitivity, SNR, and Q-factor .....	31
2.4.5.1 Sensitivity .....	31
2.4.5.2 Signal to noise ratio .....	33
2.4.5.3 Quality factor .....	34
2.4.6 Measurement techniques .....	34
2.4.6.1 Scattering parameters .....	34
2.4.6.2 Smith chart .....	36
2.4.6.3 Tools and methods .....	36
3 Materials and Methods .....	39
3.1 Design Considerations on Test Prototype .....	39
3.1.1 Coil geometry .....	40
3.1.1.1 Estimating the total size of the coil .....	40

3.1.1.2	Size of the test loop and array .....	41
3.1.2	Tuning and matching .....	42
3.1.3	Mutual decoupling .....	45
3.1.3.1	Transformer decoupling .....	46
3.1.3.2	Overlap decoupling .....	47
3.1.3.3	Preamplifier decoupling .....	48
3.1.4	Transmission decoupling .....	50
3.2	8-channel Coil Array Construction .....	51
3.2.1	Coil housing .....	51
3.2.2	PCB design .....	55
3.2.2.1	PCB manufacturer and material .....	55
3.2.2.2	PCB specifications .....	55
3.2.2.3	Schematic circuitry of the coil .....	56
3.2.2.4	PCB drawing .....	57
3.2.3	Coil construction .....	60
3.2.3.1	PCB preparation .....	60
3.2.3.2	Single channel development .....	62
3.2.3.3	Array development .....	62
3.2.3.4	Overlapping .....	64
3.2.3.5	Optimizing the channels .....	64
3.2.4	Interfacing to the MR scanner .....	66
3.2.4.1	Scanner cable connection .....	66
3.2.4.2	Cable trap .....	66
3.2.4.3	Transmit coil adjustment .....	68
3.3	Performance Testing .....	69
3.3.1	Bench tests .....	69
3.3.1.1	Tuning and matching .....	69
3.3.1.2	Inter-element decoupling .....	70
3.3.1.3	Transmission decoupling .....	70
3.3.1.4	Q-factors .....	70
3.3.1.5	Metal shield test .....	72
3.3.2	MR measurements .....	72
3.3.2.1	MR scanner .....	72
3.3.2.2	Micro-gradient system .....	72



3.3.2.3	MR experiments .....	73
3.3.2.3.1	MR experiment 1: Homogeneous cylindrical saline phantom ...	73
3.3.2.3.2	MR experiment 2: Asparagus .....	74
3.3.2.3.3	MR experiment 3: Resolution phantom .....	74
4	Results .....	75
4.1	Bench Measurement .....	75
4.1.1	Tuning and matching .....	75
4.1.2	Estimating the Q-factor .....	76
4.1.3	Influence of metal shield .....	77
4.1.4	Transmission decoupling .....	77
4.1.5	Preamplifier decoupling (PCB array) .....	77
4.1.6	Mutual decoupling (test prototype, PCB array) .....	78
4.1.6.1	Mutual decoupling of test prototype .....	79
4.1.6.2	Mutual decoupling of separate rows on the PCB .....	79
4.1.6.3	Mutual decoupling of the 8 channel receive-only coil 1 .....	80
4.1.6.4	Mutual decoupling of the 8 channel receive-only coil 2 .....	81
4.2	MR Measurements .....	82
4.2.1	Experiment 1: Homogeneous cylindrical saline phantom .....	82
4.2.2	Experiment 2: Asparagus .....	84
4.2.3	Experiment 3: Resolution phantom .....	85
4.2.4	Experiment 4: Parallel imaging performance .....	87
5	Discussion and Outlook .....	89
5.1	Discussion .....	89
5.2	Conclusions and suggestions for further work .....	90
6	Appendix .....	91
6.1	Bibliography .....	91
6.2	List of Figures .....	93
6.3	List of Tables .....	95
6.4	Publication List .....	96
6.5	Curriculum Vitae .....	96



# Abstract

High resolution magnetic resonance imaging (MRI) strongly depends on the availability of highly sensitive radio frequency (RF) coils. The goal of this work is the development of a receiver coil array with high sensitivity and parallel imaging performance.

We designed and constructed a tube-shaped eight-channel receive-only array. The inner and outer diameter of the coil tube is limited by the space available in the transmit coil and the desired sample diameter, respectively. The individual coil elements were arranged to cover the surface of the inner cylinder in two rows consisted of four elements. Elements within one row were mutually decoupled by transformer decoupling. Decoupling between rows was achieved by coil overlap. In addition, preamplifier decoupling was implemented. A double-layer flexible printed circuit board (PCB) was designed for each of the two rows. The coil conductors were deposited on one layer, the other layer contained solder pads for the circuitry required for tuning, matching, transformer decoupling, active detuning, and preamplifier decoupling. These PCBs were wrapped around the inner cylinder (phenolic paper) before soldering the components and could be moved with respect to each other to optimize overlap decoupling between the rows. Preamplifiers are placed directly at the coil to minimize losses.

Performance of the coil was validated with bench and imaging measurements. Each element was successfully tuned to 297.2 MHz and matched to  $75 \Omega$ . Efficient mutual decoupling ( $< -14$  dB) was achieved by transformer and overlap decoupling and supplemented by preamplifier decoupling ( $< -17$  dB). Active detuning circuits provided an isolation  $> 40$  dB between tuned and detuned state. A very good homogeneity over a large field of view (FOV) ( $> 90$  mm) was achieved with different samples. Construction of the array has potential for applying parallel imaging ( $R=2$ ) with a reasonable SNR. The use of thin flexible PCBs enables the incorporation of the coil circuitry and on-board preamplifiers despite the limited available space. Comparative investigations can be done between the receiver coil and other available coils for further evaluations.



# 1 Introduction

Magnetic resonance microscopy (MRM) is based on the same physical principles as MRI. MRI usually offers spatial resolutions in the order of 1 mm<sup>3</sup>. Resolution can be improved by using higher field strength, stronger gradients, and more sensitive RF coils [1].

An RF receiver coil or antenna is the first element to detect the MR signal from the sample and to transfer it to the scanner for further processing and constructing the final MR image. This antenna is tuned to work at a specific frequency called Larmor frequency.

RF coil, in its exciting role deposits an amount of energy to the sample, thus transferring spins from the lower to the higher energy levels. After excitation, the same RF coil can act as a receiver to collect the generated signal from the sample. In MRI, transmitter and receiver can share a same hardware because they do not work at the same time and in fact, they are both tuned to operate at the same frequency.

By using smaller individual coil elements for the receiver coil, the sensitivity is improved at the cost of a smaller FOV. This limitation can, however, be overcome by placing multiple of these smaller elements, covering the large FOV of a larger coil, but with the advantage of increased sensitivity and the possibility to speed up the measurement by parallel imaging techniques [2, 3, 4]. In this work, an ultra-high field MR scanner (Magnetom 7T MRI, Siemens AG, Erlangen, Germany), a dedicated strong micro-gradient system (Resonance Research, Inc., Billerica, MA, United States), and a birdcage transmit RF coil (<sup>1</sup>H 297 MHz, Rapid Biomedical, Rimpar, Germany) are available.

By combining the existing set of hardware with a new receive-only RF coil array, it will be possible to increase the signal detection sensitivity and speed considerably over previous hardware.



# 2 Basic Principles

## 2.1 MRI Physics

To understand the principles of the MR technology, many terms which are based on classical physics and quantum mechanics have been reviewed in different books, but this chapter tries to explain at least some of them to build an overall overview about the basics of MR.

In general, a subject is put in the MR scanner and radio waves are transmitted for a few milliseconds. When the transmitter is turned off, re-transmitted waves – the MR signal – are received from the subject. This signal has the same frequency as the transmitted waves. After that, the measured RF data is converted to images. The main required hardware components are a strong static magnetic field, magnetic field gradients, shims, RF coils, and computers that manage the timing and control all the components [2, 3, 4].

MRI measures the net magnetization of atomic nuclei in the presence of an external magnetic field  $B_0$ . Protons and neutrons have an intrinsic angular momentum (spin) quantum number  $\frac{1}{2}$ . Because of the Pauli principle, spin up and down nucleons pair up and the overall spin cancels out. Therefore, odd number of protons or odd number of neutrons in the nucleus of an atom results in a non-zero total nuclear angular momentum  $I$ . Its magnitude can only take the values

$$|I| = \hbar\sqrt{I(I + 1)} \quad \text{Eq. 1}$$

For the  $^1\text{H}$  nucleus (i.e. a single proton),  $I = \frac{1}{2}$ , this results in  $|I| = \frac{\sqrt{3}}{2}\hbar$ . The projection of the total nuclear angular momentum in a direction  $z$  is also discretized:  $I_z = m_z\hbar$ , described by the secondary spin quantum number  $m_z$  with allowed values between  $-I$  and  $+I$  in steps of 1; in the case of  $^1\text{H}$ , these are  $-\frac{1}{2}$  and  $+\frac{1}{2}$ .

Associated with the spin is a magnetic moment  $\mu$ , it is collinear and proportional by a factor  $\gamma$ , called the gyromagnetic ratio:

$$\mu = \gamma I \quad \text{Eq. 2}$$

Without external magnetic field, the directions of the nuclear spins, and therefore, the magnetic moments, are randomly oriented in space. When an external magnetic field  $B_0$  is applied, the spins align with the field, pointing either in the same direction (parallel) or in the opposite direction (anti-parallel) to  $B_0$  (Fig. 1a). The potential energy of a magnetic moment along the direction of a magnetic field in z-direction (without loss of generality) is  $E = -\boldsymbol{\mu}\mathbf{B}_0 = -\mu_z B_0$ , resulting in splitting of the energy levels for the different quantum states of the nucleus for  $B_0 > 0$ . This effect is called Zeeman-splitting (Fig. 1b) [2, 3, 4].

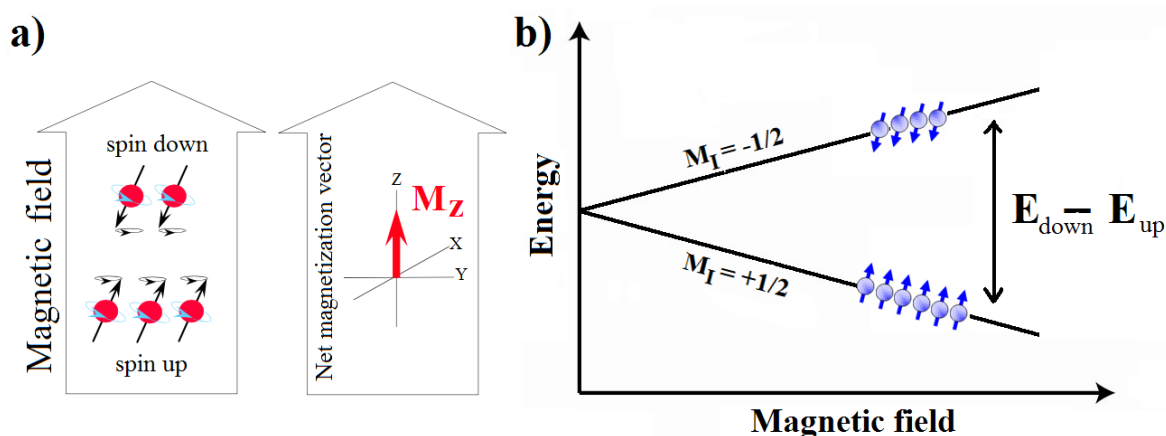


**Figure 1: Basics of magnetic resonance imaging.**

**a) Spins in a magnetic field. b) Zeeman effect.**

The spins which are aligned parallel to the direction of the applied magnetic field, have the lower energy. Spins which aligned anti-parallel to the applied magnetic field, have the higher. In thermal equilibrium, the number of spins in the lower energy level  $n_+$  will be higher than the number of spins  $n_-$  in the higher energy level. Boltzmann distribution explains that this excess in population rate depends on the temperature  $T$  and the strength of  $B_0$ :

$$\frac{n_+}{n_-} = \frac{e^{-\frac{E_+}{k_B T}}}{e^{-\frac{E_-}{k_B T}}} = e^{\frac{E_- - E_+}{k_B T}} = e^{\frac{\Delta E}{k_B T}} = e^{\frac{\gamma \hbar B_0}{k_B T}} \quad \text{Eq. 3}$$

with  $\gamma$  the gyromagnetic ratio, and  $k_B$  Boltzmann's constant.

At physiological temperature (310 K), this corresponds to 5 spins per million at a field strength of 1.5T, 10 at 3T, and 23 at 7T, respectively. This is the net macroscopic magnetization usable for MR experiments. In typical human tissue there are about  $3 \times 10^{28}$  protons per  $\text{m}^3$ , so there are approximately  $3 \times 10^{15}$  spins contributing to the MR signal in a



typical 5 mm<sup>3</sup> measurement volume at 7T, or below 7x10<sup>11</sup> in MR microscopic experiments with less than (100 μm)<sup>3</sup> voxels [2, 3, 4].

Using  $\mu_z = \gamma I_z$  and  $I_z = m_z \hbar$ , the potential energy eigenvalue for a given state  $m$  is  $E_m = -\gamma m_z \hbar B_0$ . For <sup>1</sup>H,  $m_z = \pm 1/2$ , therefore the energy difference between the two possible states is  $\hbar \gamma B_0$ . A photon has the same energy as this energy difference when  $\hbar \omega = \hbar \gamma B_0$ , leading to the Larmor equation

$$\omega = \gamma B_0 \quad \text{Eq. 4}$$

where  $\omega$  is called the Larmor frequency, which is in the RF range for commonly employed  $B_0$  in the range of a few Tesla. Irradiating the spins with radio waves of exactly this frequency causes transitions from the lower to the higher energy state of the spins. This phenomenon is called nuclear magnetic resonance (NMR). The spin system tends to return to the thermal equilibrium, and releases the acquired energy by emitting itself photons at the Larmor frequency – this is the MR signal which can be detected by a so-called RF coil.

The total magnetic field in an MR scanner is created by the sum of the main field  $B_0$  (usually generated by a helium-cooled superconducting magnet), shim fields for homogenizing the static field, and gradient fields.

Gradients are additional magnetic fields which vary over space, causing a spatial dependence of the total field, on the position in the magnet bore. According to the Larmor equation this results in different precessional frequencies and therefore the MR signal from the subject can be attributed to a certain location in space via spectral analysis, i.e. Fourier transform (Fig. 2). During a typical MRI scan, gradients are changed very quickly and repeatedly which cause to produce the acoustic noise of MRI [2, 3, 4].

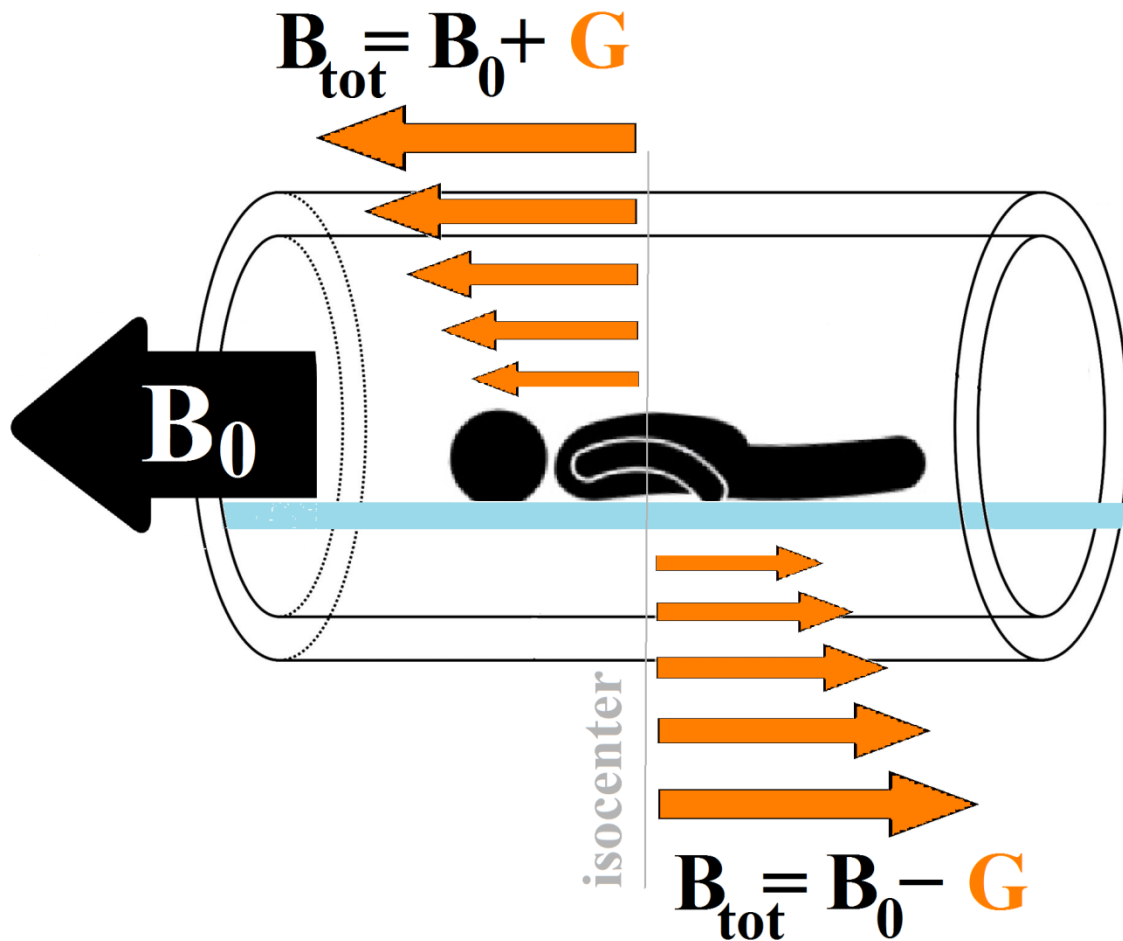


**Figure 2: Dependency of the magnetic field to the position.**

Finally, to receive and transmit the radio waves to the spins, RF coils are needed, which will be discussed in detail later.

The MR sensitivity for a certain nucleus depends on various factors; having a non-zero nuclear spin, a higher abundance of the target nucleus in biological tissues, and a higher gyromagnetic ratio. The hydrogen atom  $^1\text{H}$  has the most sensitive nucleus in MRI because of its high natural abundance and gyromagnetic ratio. Commonly used isotopes other than  $^1\text{H}$  are  $^{13}\text{C}$ ,  $^{19}\text{F}$ ,  $^{31}\text{P}$ , and  $^{23}\text{Na}$  (Table 1). All of these elements precess at a specific Larmor frequency, thus to detect them, RF coils that are tuned to resonate at their specific Larmor frequencies, are applied. For instance, in a 1.5 Tesla scanner,  $^1\text{H}$  and  $^{13}\text{C}$  resonate at 63.86 MHz and 16.05 MHz, respectively [2, 5].

**Table 1: Important magnetic resonance properties of useful nuclei [5]**

Nuclear isotope	Natural abundance (%)	$\gamma / 2\pi$ (MHz/T)
$^1\text{H}$	99,98	42,58
$^2\text{H}$	0,015	6,53
$^7\text{Li}$	92,6	16,5
$^{13}\text{C}$	1,11	10,71
$^{14}\text{N}$	99,6	3,1
$^{19}\text{F}$	100	40,05
$^{23}\text{Na}$	100	11,26
$^{31}\text{P}$	100	17,23
$^{39}\text{K}$	93,1	2

## 2.2 High Field MRI

Usually, an MRI scanner with field strength above 1.5T is considered as a high field. High field MR brings several benefits for research and clinical application. Higher MR signal due to the higher magnetization can be traded for higher spatial resolution, shorter imaging time, or better signal-to-noise ratio (SNR). Also, in MR spectroscopy, better spectral resolution due to stronger chemical shift is an advantage of high field MRI. At higher field, so-called X-nuclei (all nuclei other than  $^1\text{H}$ ) such as  $^{31}\text{P}$  and  $^{23}\text{Na}$  can be more easily detected. On the other hand, high field MR has some technological, physical and safety limitations. In particular, limitations include homogeneity of the static magnetic field  $B_0$  and the RF field  $B_1^+$ , changes in relaxation kinetics, increased susceptibility effects, higher deposited power from RF pulses in the tissue (=specific absorption rate, SAR). These limitations increase the complexity of such scanners. As a result, higher  $B_0$  is more expensive in terms of size, weight, and cost. High field and ultra-high field ( $\geq 7\text{T}$ ) scanners are usually 3T, 4.7T, 7T, 9.4T, and 11.7T (corresponding to  $^1\text{H}$  frequencies of 125, 200, 300, 400, and 500 MHz, respectively).

Between 1999 and 2016, around 70 units of 7T human scanners have been installed worldwide by main manufacturers of MRI such as GE, Philips, and Siemens. Usually, the bore sizes of such scanners are between 68 and 90 cm [6, 7, 8].

## 2.3 MR Microscopy

Since the 1990s, with the development of the technology of magnets, RF coils, and pulse sequences, the use of MRM has rapidly grown. MRM is defined as MRI at microscopic levels with resolutions better than  $100 \mu\text{m}^3$ . This noninvasive method to study biological samples allows scientists to have a volumetric view of a sample which is in some cases at ultra-high fields comparable with histopathology.

MRM benefits from stronger gradient systems (10 to 20 times stronger). This can only be achieved by using a smaller bore size, however limiting the measurement to smaller samples. Improving spatial resolution means reduction of the voxel size and leads to proportionally weaker acquired signal. This means that sensitivity is the most important issue in MRM. Designing more sensitive RF coils therefore helps to improve spatial resolution and SNR [1, 9].

## 2.4 Radio Frequency Coils

### 2.4.1 General aspects

The first important issue to know is that the RF signal is not due to the emission of radio waves by nuclei. Instead, it is a current which induced by the net magnetization vector of the spins. According to the Faraday's law, not only the electrical currents produce a magnetic field, but also changing magnetic fields induce electrical currents. MR signal is based on this finding. As soon as the magnetization vector tilts from its equilibrium, it starts to precess around the  $B_0$  in order to be relaxed again. This precession motion, which has a constant frequency, causes changes in magnetic flux in a loop of wire and therefore produces current and a detectable voltage in the wire. The simplest form of a receiver coil to detect the MR signal is a single loop of conducting material signal [2, 5].

During the relaxation, every time that the magnetization vector passes the smallest distance from the receiver, the intensity of this signal becomes maximum. Conversely, the further the vector goes away from the receiver, the less signal intensity is detected. Moreover, magnetization or signal intensity vanishes after a certain time but its frequency remains constant. As a result, the relaxation forms a signal in receiver coil which is called free induction decay or FID (Fig. 3) [5].

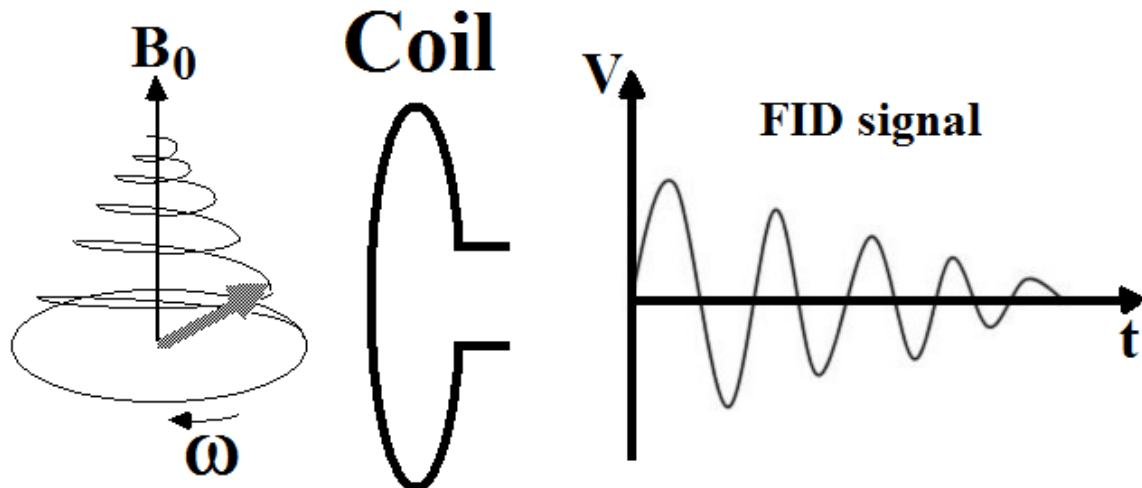


**Figure 3: Free induction decay.**

The detected signal is then amplified, digitized and processed for further steps which result in construction of the final MR image. In most modern scanners and almost up to 3 T, RF transmission and reception functions are separated with different hardware. Nevertheless, in high-field MR scanners which do not have a body RF transmission coil, the transmitter and receiver are often integrated into one coil with an additional circuitry (T/R Switch) to ensure the correct performance of the transmitter and receiver [2, 5]. By now based on the function of the RF coils, they can be categorized into 3 different types:

- Transmit only (TX)
- Receive only (RX)
- Transmit and Receive (Transceiver, TRX)

Receiver coils are grouped into two main classes: surface and volume coils.

Simply a loop of wire either rectangular or circular is considered as a surface coil. These types of coils are designed based on this fact that the closer the receiver is placed to the region of interest (ROI), the stronger the signal is detected. Surface coils increase the SNR and sensitivity of the coil which is inversely related to the size of the coil. Due to the size limitation of a typical single surface coil, it can only cover a small part of the anatomy. To overcome this problem, phased array coils, which are a group of surface coils to cover a larger FOV like spine, are widely used.

To have a maximum efficiency and penetration of the RF energy, volume coils are designed in form of quadrature. Typically, a quadrature coil is consisted of two separate

coils each oriented at  $90^\circ$ . The signal from both coils is simultaneously recorded at different phases (Sine and Cosine). Volume coils have different forms like paired saddle coil and birdcage coil which is widely used in MRI applications of head and knee (Fig. 4) [5].

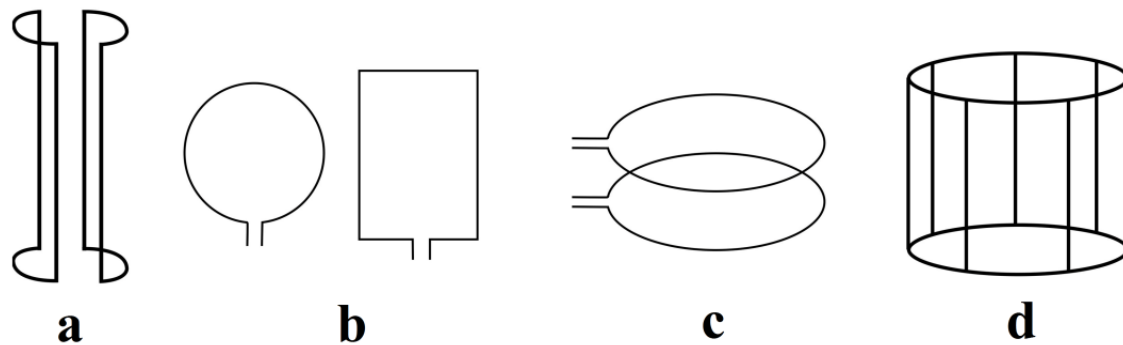


**Figure 4: Different types of coils. a) Paired saddle coil. b) Surface coils. c) Helmholtz pair coil. d) Birdcage coil.**

(Source: Case courtesy of A. Prof Frank Gaillard, Radiopaedia.org, rID: 21753)

Designing a good receiver coil needs some factors to ensure that the signal is recorded at the correct frequency with the maximum efficiency. However, an important considerable issue is that the receiver coil must be deactivated while the transmitter works [1, 2]. Therefore, the important designing factors for receiver coils are explained in further sections.

### 2.4.2 Tuning and matching

Generally, an RF coil is estimated with an RLC circuit which resonates at the reference frequency,  $\omega_0$  (Fig. 5). Since the inductance  $L$  and resistance  $R$  of the coil are determined by the geometry of the coil, capacitance  $C$  is the only adjustable parameter in this RLC circuit to make the resonance at Larmor frequency when  $\frac{1}{LC} = \omega^2$ . The impedance of a loop of wire, which is tuned at Larmor frequency by a capacitor, will be  $Z = R + jX$ . In order to transfer the MR signal to the further electronic circuitry with the maximum efficiency and the minimum of loss, the impedance of the coil should be matched as closely as possible with the cables, transmission lines and input of the preamplifiers. In most of the cases, this impedance is set to  $50 \Omega$ . Any mismatch in between causes inefficient signal intensity and a poor image quality [10].

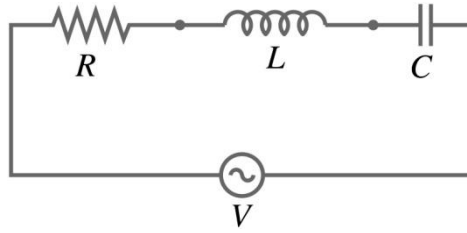


**Figure 5: Equivalent electrical circuit of a receiver coil.**

As a result, a coil is consisted of a loop of conducting material with one or more capacitors to operate at Larmor frequency and to increase the resistance to 50  $\Omega$ . It has been reported that the R of a coil is much less than 50  $\Omega$ . Also, a coil has one or more compensating capacitors to make it match and reduce the reactance ( $jX$ ) of the coil to zero. Fig. 6 shows a typical configuration of a single coil with tuning and matching capacitors [5, 10].

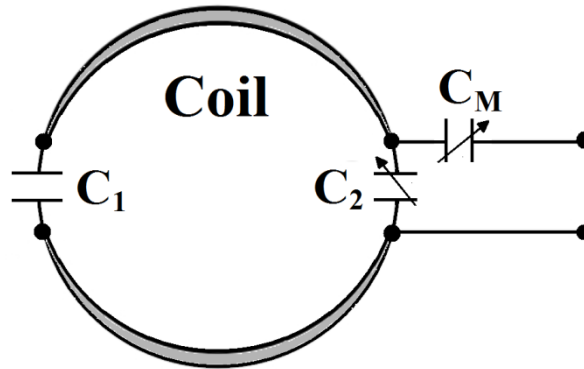


**Figure 6: A simple receiver coil with tuning and matching elements.**

Tuning means choose a compatible capacitor with 50  $\Omega$  and tune it with the coil to operate at the exact desired frequency. Matching means choose another capacitor to connect in the output of the coil, which adjusts the output resistance to 50  $\Omega$  while converts the output reactance to zero. When tuning, the impedance is

$$Z = R + jX = \frac{1}{\frac{1}{r+jL\omega} + jC\omega} \quad \text{Eq. 5}$$

In Fig. 7, black box indicates the requirements of a matching network to fulfill the desired impedance [10].

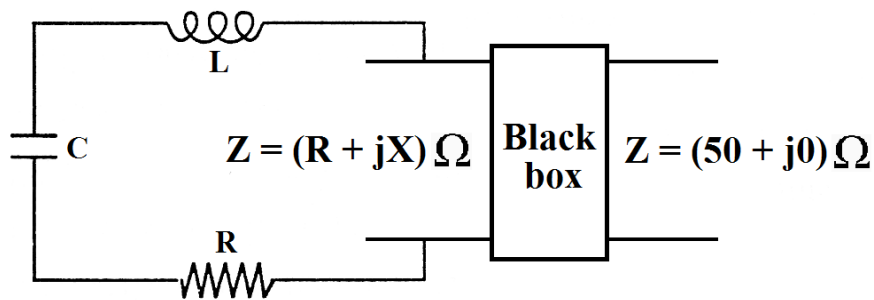


Figure 7: Function of the matching network.

### 2.4.3 Transmission decoupling

In RF receiver coils, one important challenge which should be treated carefully is transmission decoupling. During the excitation phase of the nuclei, a large amount of energy is transferred from the RF transmitter into the sample. This powerful energy can potentially damage the receiver coils and their preamplifiers. To prevent the receiver coil from hundreds of Watts of RF power, an additional circuitry should be designed to ensure that high power pulses do not destroy the receiver coil. Transmission decoupling is based on this idea that the both receiver and transmitter are tuned at the same frequency. Therefore, to prevent the receiver coil, it suffices to change the operating frequency of the receiver coil during the transmission phase. A circuitry can be designed to readjust the frequency very quickly in receive mode.

Conceptually, an LC trap which is tuned at  $\omega_0$  should be placed on the receiver circuitry to work simultaneously with the transmitter. During transmit mode,  $L$  is connected to the  $C$  either passively or actively to resonate at  $\omega_0$  and thus to detune the receiver coil and to protect the elements. Fig. 8 shows the coupling and decoupling situations in different operating modes [11].

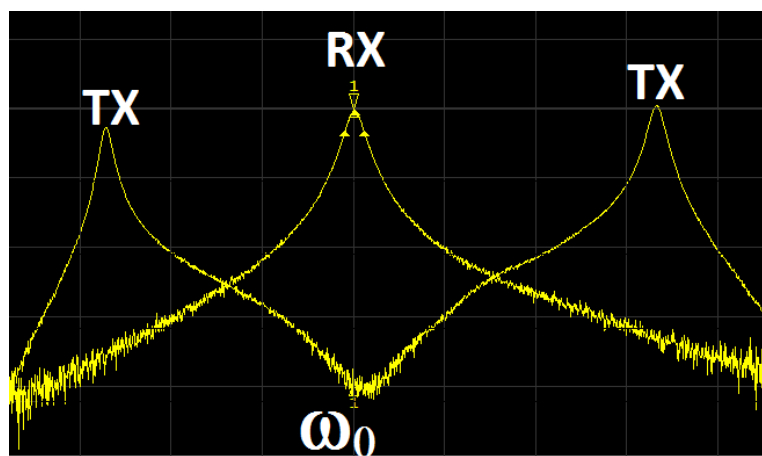


Figure 8: Tuning and detuning in receive and transmit modes.



Two methods for transmission decoupling have been suggested, passive and active decoupling. Both methods have the ability of fast switching by using diodes between receive and transmit modes.

### 2.4.3.1 Passive decoupling

This method is based on the non-linearity of current-voltage characteristics of diodes. Every diode has a cut-off voltage. When the voltage across the diode becomes larger than a certain limit, it presents a low resistance and makes a short circuit. Instead, when the diode is reverse-biased, it presents a very high resistance and acts as an open circuit. So depending on the applied voltage, diode behaves like a switching device (Fig. 9) [11].

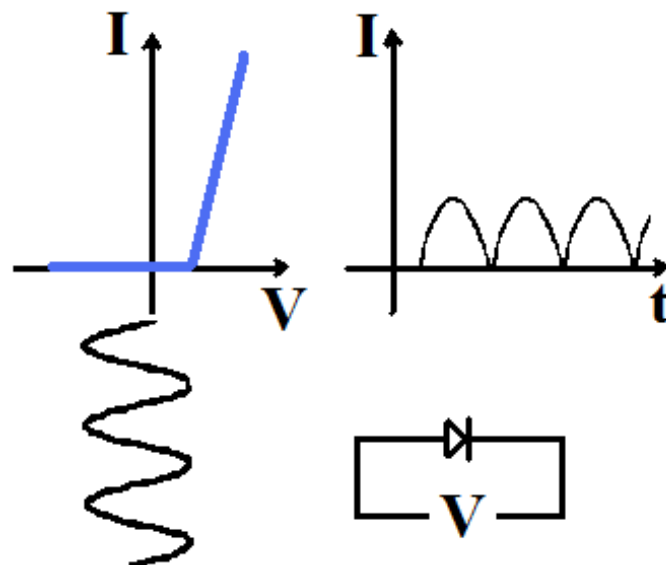
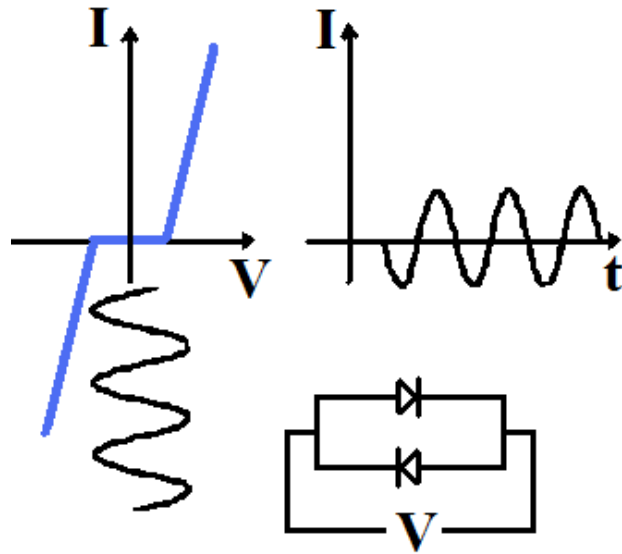


Figure 9: Voltage-current characteristic of one diode.

In passive decoupling, no external voltage is used to bias the fast RF diode. On the other hand, one single diode passes only a half of the RF current resulting in a large power loss. Therefore, to have a better performance of the switching and to avoid shape distortion of the RF current, a second diode should be inversely connected to the first one. Fig. 10 explains the function of the diodes during transmit mode [11].



**Figure 10: Voltage-current characteristic of two diodes in passive decoupling.**

### 2.4.3.2 Active decoupling

As with the previous method of decoupling, diode is also the main element in this method. Instead of the fast RF diodes, a PIN diode is used because it has a better performance than the fast RF diodes. To have forward- and reverse-biased, a PIN diode must be activated through an external source of power. When PIN diode is forward-biased, it acts as a short circuit due to its small resistance ( $0.1 \Omega$ ). When it is reverse-biased, it acts as an open circuit because it presents a high resistance of about  $200 \text{ K}\Omega$ . The external source of power works synchronously with the transmitter to ensure that whenever the transmitter is turned on the PIN diode will be also turned on to decouple the receiver coil and to protect it. In receive mode, the PIN diode is deactivated and through a so-called RF choke it isolates the receiver coil from additional noisy resistance and preserving the electrical balancing of the circuit (Fig. 11). In principle, chokes are used to block the AC while passing the DC [11].

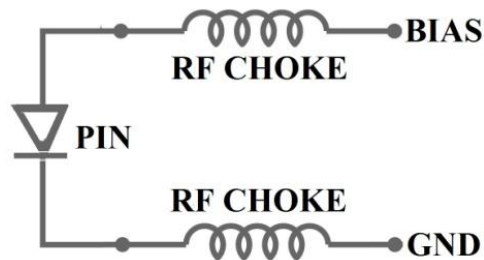


**Figure 11: Circuit diagram of the active decoupling.**

## 2.4.4 Coil arrays

Fig. 12a shows how a part of the sample volume is covered by a surface coil. Size of a surface coil is limited because its sensitivity is inversely proportional to the radius of the coil. Since this limit results in a smaller element and therefore covering a smaller FOV, phased array construction can solve the problem. A phased array coil is consisted of several independent small coil elements to capture the MR signal from a larger volume with the advantages of high spatial resolution, a larger FOV, and SNR improvement [12]. Fig. 12b shows four separate surface coils in an array which are placed with  $90^\circ$  phase difference.

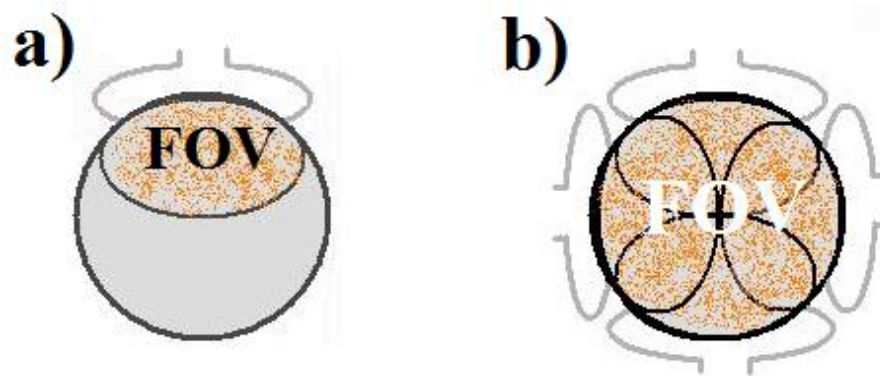


**Figure 12: Field of view by different coils.**  
a) Single surface coil. b) Phased array coil.

### 2.4.4.1 Mutual decoupling

In electronics, wanted or unwanted transfer of energy from one medium calls coupling. Mutual coupling in the theory of antenna defined as unwanted energy absorbed by one antenna when another antenna is operating. Specifically, any kind of disturbances which degrade the efficiency of an antenna or a circuit called electromagnetic interference (EMI). In order to reduce this effect, mutual decoupling defined as the reduction of undesired interferences to prevent the antennas [13].

In MRI, RF coils work in near fields and they must be placed within some other coils e.g. gradients, and shims which can increase the EMI. On the other hand, the EMI as well as mutual coupling are significantly increased when a receiver coil is consisted of arrays. In an array, each antenna element is tuned to the Larmor frequency and is located close to other elements. These factors induce a strong coupling and degrade the efficiency of the coil. Therefore, every individual coil element must be isolated from other elements

otherwise elements will interact with each other which causes mixing the signal from different positions of the sample [6].

Different types of decoupling methods for array elements have been investigated by scientists. Among them are three methods which are applied most common and were used in this work.

#### 2.4.4.1.1 Overlap decoupling

This method is applied for the adjacent coil elements. Since the mutual coupling between coils is in the form of mutual induction, which makes a linkage in magnetic flux, sharing some parts of adjacent coils cancels out the magnetic flux in the common area through the non-overlapping areas. Fig. 13 demonstrates the influences of mutual coupling and overlapping on the signal. This method can be also used between two different arrays which have similar configurations [6, 14].

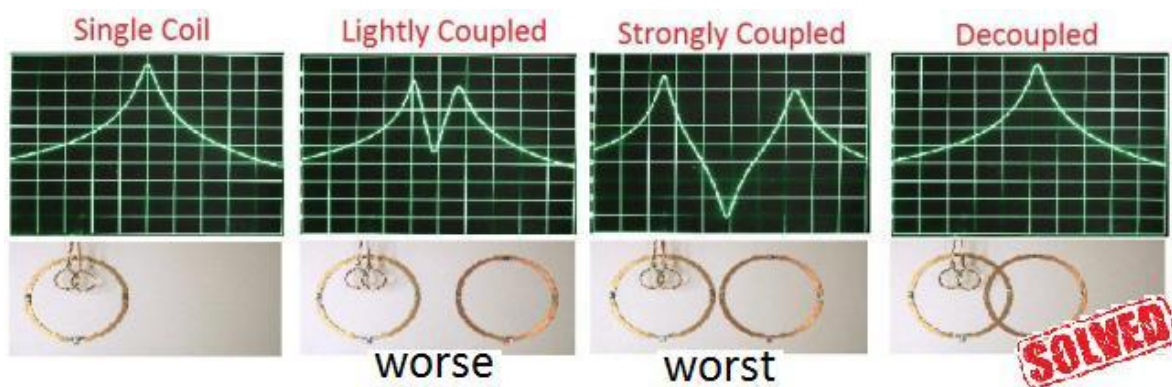


**Figure 13: Effect of overlapping on mutual coupling.** (Source: NYU School of medicine)

#### 2.4.4.1.2 Capacitive and inductive decoupling

These methods are used for both adjacent and non-adjacent coil elements. Inductive decoupling or transformer decoupling is similar to overlapping due to the physical principles. In fact, one small inductor coil is connected to a large imaging coil to share the common area with another small inductor from an adjacent or non-adjacent imaging coil and thus to cancel out the magnetic flux. These two small inductors are placed very close to each other in order to counteract the mutual coupling with mutual coupling of their imaging coils. The advantage of this method is that the adjustment of small inductors to have a very good isolation is easy.

Capacitive decoupling is a network which uses capacitors instead of small inductors. The values of the capacitors in the network reduce the mutual coupling between adjacent or non-adjacent coils [14, 15].

#### 2.4.4.1.3 Preamplifier decoupling

Another function of the preamplifiers is to reduce the mutual coupling and interaction between the either adjacent or non-adjacent coil elements. Low noise input preamplifiers are designed to increase the coil isolation and simultaneously to amplify the first detected MR signal (order of  $\mu\text{V}$ ) before it goes to the cables for further processes. This kind of preamplifier should be placed as close as possible to the coil element [14].

A matching network must be placed between a preamplifier and a coil to fulfill two important conditions at the same time. It should not only provide a proper impedance matching (typically  $50\ \Omega$ ) but also should transfer the input impedance of the preamplifier to a very large impedance (Fig. 14). This is basically done because the large impedance effectively limits the current flowing through the coil and therefore minimizes the mutual coupling. However, it reduces the MR signal power but for modern preamplifiers, it is still a good method to improve the isolation. In general, preamplifiers with a high reflection coefficient ( $r$ ) at the input possess a very good SNR [14, 16, 17].

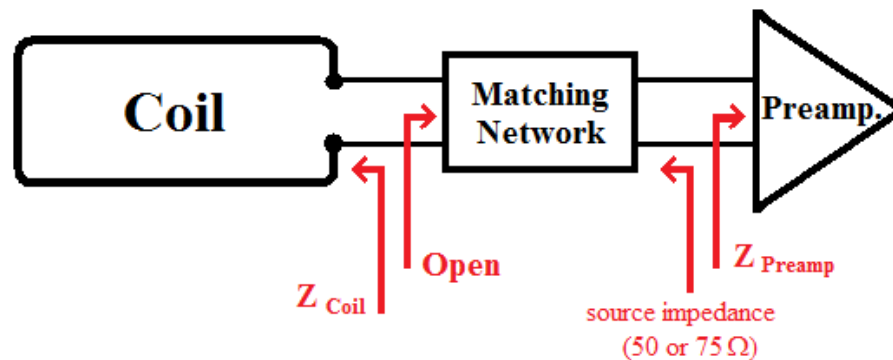


**Figure 14: Concept of preamplifier decoupling.**

Matching networks are usually two or more reactive elements with the minimum of losses which are arranged in different configurations. Indeed, a matching network for preamplifier decoupling is consisted of a decoupling network and a matching network, but in general, all together are called matching network. During the reception, this network is responsible for transferring the detected MR signal with the maximum efficiency to the preamplifier which can be placed either close to the coil or in distance.

Usually, the input impedance of the preamplifiers is set to 50  $\Omega$ , however, in some modern preamplifiers this impedance can take other values which is not 50  $\Omega$ .

One challenge is to choose a proper combination of reactive elements for the matching network. In order to design such a matching network, four different configurations have been suggested by Reykowski et al. which can be used for low noise preamplifiers [17]. Input impedance of the preamplifier, which is measured by its manufacturer and mentioned in its datasheet, has an important role to define the elements of the matching network. The input impedance of such preamplifiers can be either close to a short circuit or close to an open circuit. Usually, the input impedance of the preamplifiers is assessed with  $r$ , which is the ratio of the reflected signal divided by the incident signal. For an ideal case the following relations are valid:

$$\begin{aligned} & \text{if } r = 1 \angle 0^\circ, \text{ then} \\ & \text{Impedance } Z = \infty \equiv \text{open circuit} \end{aligned}$$

$$\begin{aligned} & \text{if } r = 1 \angle 180^\circ, \text{ then} \\ & \text{Impedance } Z = 0 \equiv \text{short circuit} \end{aligned}$$

#### 2.4.4.2 Parallel imaging

A faster imaging time needs receiver coil arrays and parallel imaging. Parallel imaging uses a simultaneous data acquisition from every single coil in an array. By now, many different pulse sequences, which are based on reducing the number of K-space lines, have been suggested by scientists in order to reduce the imaging time in MRI. One drawback of the parallel imaging is that the SNR suffers from two factors which are not in conventional imaging. Therefore, SNR of an image which is measured by parallel imaging can be lower than the same image which is measured by non-accelerated imaging methods. It has been mentioned that the SNR in parallel imaging can be achieved by

$$SNR_{parallel} = \frac{SNR}{g\sqrt{R}} \quad \text{Eq. 6}$$

Where  $g$  is the geometry factor and  $R$  is the reduction or acceleration factor. For instance, if the speed of the imaging time is increased by factor of 2, then the SNR will be decreased by factor of  $1/\sqrt{2}$ , which means 30% reduction in SNR. The speed of the imaging is increased because only  $\frac{1}{R}$  of the k-space are filled with MR data. Instead, G-factor depends on the geometry of the receiver coil, e.g. location of the channels and

the coil loadings. This factor is one of the hardware limitations which restricts the acceleration factor and reduces the SNR. Specifically, when the adjacent coils are highly correlated to each other, the aliased pixels will be hard separated. Usually, acceptable values for g-factor are between 1 and 2 [18, 19].

## 2.4.5 Sensitivity, SNR, and Q-factor

### 2.4.5.1 Sensitivity

As has been mentioned earlier in the basic principles of MR, high-field MR has some advantageous that among them sensitivity plays an important role. There are many factors to increase the sensitivity of an MR image but only a few of them are related to this work. During the signal acquisition by the receiver, the information of phase and frequency gradients, which is embedded in the detected signal, are used to the spatial encoding of the final MR image. Any distortion in this information results in reduction of the image quality or even to destroy the image. Accordingly, the stability of the RF system, transmitter and receiver is very important. It has been reported that a typical RF coil should be individually designed for every application because every application has its own demands [16]. Some requirements to have an optimized RF coil are as follows:

- The coil has to be sensitive in the ROI. To avoid signal loss, essentially, detection of the MR signal is performed after excitation of the magnetization. The induced electromotive force in the receiver coil is given by:

$$emf = - \int \frac{B_1}{i} \cdot \frac{\partial M}{\partial t} dV \quad \text{Eq. 7}$$

In this equation,  $\frac{B_1}{i}$ , which is called coil sensitivity, is the magnetic field produced by the unit current in the coil at the location of M. This integral is applied over the sample's volume. Therefore, the volume, which is located under the coil element, participates in MR signal. As a result, the sensitivity of a coil is inversely proportional to its distance from the sample. In other words, to achieve a high sensitivity, the filling factor must be maximized, such that the sample occupies most of the sensing region of the coil. For example, surface coils as receive-only elements have a very good sensitivity since they are placed near the tissue. In such coils, the sensitivity is changed not only with the distance but also with the coil radius. Therefore, small surface coils, which are placed above the sample, provide

a higher sensitivity in comparison to large coils (Fig. 15) [3]. In most of the applications, phased array coils are used to cover a large FOV.

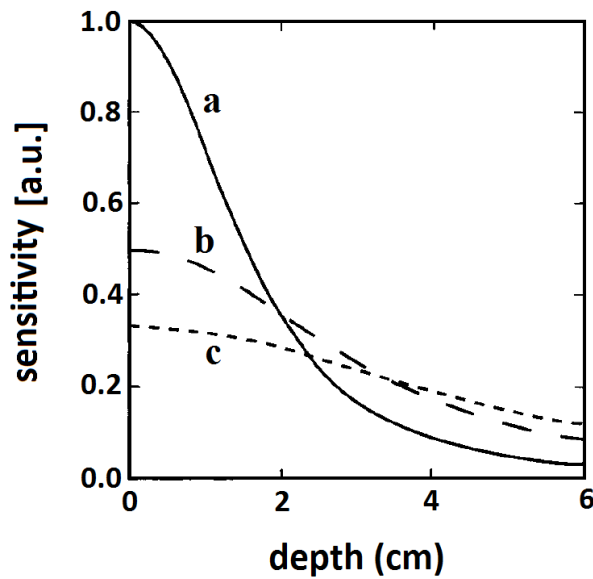


**Figure 15: Sensitivity vs. depth for circular surface coils.**

**a) Radius = 2 cm. b) Radius = 4 cm. c) Radius = 6 cm.**

- Furthermore,  $B_1^+$  homogeneity produced by the coil should be optimized. In a receive-only coil, this can be achieved by designing a good transmission decoupling circuit.
- To minimize the electric field around the coil, the length of the wires should be considered shorter than a tenth of the wavelength.
- It has been suggested that the symmetric configuration of the coils in an array can improve the sensitivity of the coil.
- To reduce the common mode currents, using the cable traps for coaxial cables can be useful to increase the sensitivity of the coil and to avoid unwanted electromagnetic couplings.
- Finally, one can take into account is the materials which are used in the construction of the RF coil. These materials can change the homogeneity of the static magnetic field  $B_0$  [3, 11, 16].



### 2.4.5.2 Signal to noise ratio

The image quality of the MR usually depends on three important parameters: spatial resolution, image contrast, and SNR. In fact, SNR describes the relationship between MR signal and the amount of the image noise. Practically, SNR is obtained from the mean signal intensity measured in an ROI over the standard deviation of the signal intensity in a region outside of the anatomy or sample, where no tissue signal exists [14]. More specifically, SNR can be expressed as

$$SNR \cong \frac{\omega_0^2 \cdot \left(\frac{B_1}{i}\right) \cdot V_s}{\sqrt{R_{noise}}} \quad \text{Eq. 8}$$

Where  $\omega_0$  is the resonance frequency that is directly increased by increasing the field strength,  $B_1/i$  is the coil sensitivity,  $V_s$  is the sample volume, and  $R_{noise}$  is the noise resistance of the sample and the coil [1]. In MRI, the goal is to increase the SNR. A variety of factors such as imaging parameters and coil characteristics affect the signal and sensitivity. Some of factors are briefly listed in Table 2 [5].

**Table 2: Parameters to improve the SNR**

Increase signal	Increase sensitivity
Larger voxel volume (lower matrix, thicker slice)	Decrease receiver bandwidth
Optimize image (short TE, long TR)	Optimize coil (surface coil, phased array)
Higher field strength	

On the other hand, SNR can be degraded by noise. In fact, any electronic manipulation adds unavoidable noise or random voltages to the detected signal. This can be seen in magnetic field inhomogeneities, thermal noise from the RF coils and patient-related factors such as body movement or respiratory.

It has been investigated that for most of the MR applications, the noise voltage, which is added to the induced MR signal, is thermal noise given by

$$N = \sqrt{4kTR\Delta v} \quad \text{Eq. 9}$$

Where  $\Delta v$  is acquisition bandwidth,  $T$  is temperature,  $R$  is magnitude of the noise resistance and  $K$  is the Boltzmann's constant. During designing the RF coils, the only adjustable factor in Eq. 9 is the total resistance  $R$ . Different parameters which can affect the  $R$  are listed as follows:

- Losses within the wires caused by the ohmic resistance of the wire.
- Losses due to magnetic interactions which are generated by fluctuation of the magnetic field  $B_1^+$  in near field during transmission.
- Losses due to electric interactions which are produced by potential differences between different parts of the coil in the near field.
- Losses due to the electromagnetic radiation which is caused by radiation of energy into the far field [16].

### 2.4.5.3 Quality factor

One important factor which must be measured during the manufacturing of the coil is the relationship between losses in the coil and the losses induced by the sample. This relationship is described by Quality factor (Q factor). A common definition for this factor is

$$Q = \frac{\omega L}{R} \quad \text{Eq. 10}$$

Where  $L$  is the inductance and the  $R$  is total resistance of the coil which has a significant effect on SNR. The goal is to achieve high values for  $Q$  which means low losses. Usually, environmental losses and an imperfect coil setup can decrease the  $Q$ . There are different ways to measure the  $Q$  but only one of them is described in detail in chapter 3.3.1.4 [10, 16].

## 2.4.6 Measurement techniques

### 2.4.6.1 Scattering parameters

To evaluate an RF coil, a common measurement technique is to apply scattering parameters (S-parameters). S-parameters are frequency dependence and describe the relationship between input and output terminals of an electrical device or device under test (DUT). A vector network analyzer (VNA) is the most convenient, but also expensive, device to measure the S-parameters.

Based on S-parameters, VNA measures the incident, reflected, and transmitted signals that are passed along the transmission lines. Principally, VNA is similar to an optical

system. When light strikes a lens, a part of the light is reflected and the most of it will be transmitted. Analogously, VNA transfer signals instead of the light and measures the incident, reflected and transmitted signals. VNA generally measures the incident signal with R or reference channel. The reflected signal is measured with channel A and the transmitted signal is measured with channel B (Fig. 16a) [20].

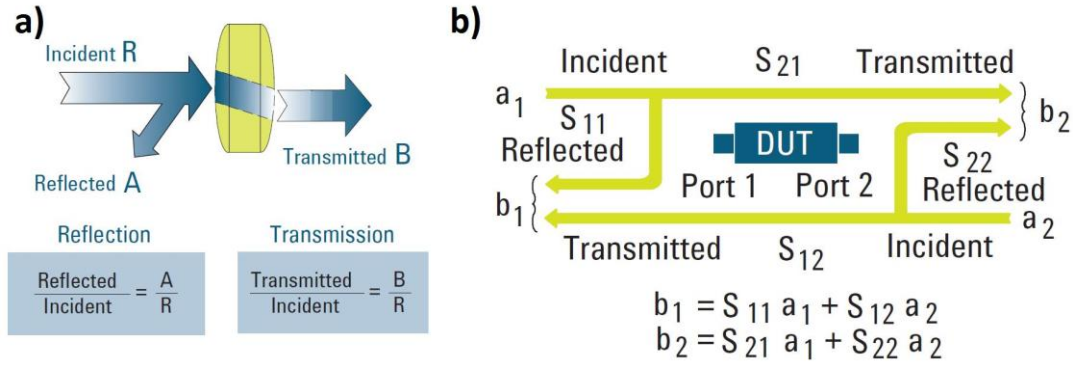


**Figure 16: Principles of scattering parameters. a) Relationships between incident, reflected, and transmitted signals. b) Equations between input and output.**

Fig. 16b shows the relationships between output and input of a DUT based on the S-parameters. For instance, to measure the isolation between two antennas, two ports are contributed to the measurement. Then  $S_{12}$  represents the power transferred from port 2 to port 1.  $S_{21}$  represents the power transferred from port 1 to port 2. Generally,  $S_{ij}$  represents the power transferred from port  $i$  to port  $j$  when  $\begin{cases} i, j = \{1, 2, \dots, n\} \\ i \neq j \end{cases}$ .

Similarly,  $S_{11}$  is the reflected power of port 1 to the delivered power to this port. As a matter of course, it is also valid for any  $S_{ii}$  when  $\{i = 1, 2, 3, \dots, n\}$ .

VNA is capable to measure the parameters at different units. But in most of the cases and preferably in MR society, the unit to express the differences and levels is decibel (dB).

Thus, the relationship between an input power  $P_{in}$  and an output power  $P_{out}$  are:

$$10 \times \log_{10} \frac{P_{out}}{P_{in}} \quad \text{Eq. 11}$$

For instance, if the output power is half the input power,  $P_{in} = 2 \times P_{out}$ , then the power ratio in decibel is -3 dB. The minus indicates that there is a power reduction. Another example can be shown in S-parameters for two coil elements. If delivered power to the first coil is 1 Watt and  $S_{21}$  is -10 dB, then it means only 0.1 Watts of power is received at the second coil [20, 21].

### 2.4.6.2 Smith chart

To measure the exact impedance of the coil elements, Smith Chart offers a very good viewing of the input impedance. It measures through the  $S_{11}$  and plots the results on a rectilinear grid known also as the complex impedance plane. Since the impedance is represented by real and imaginary parts ( $R \pm jX$ ), the resistance as real part and the reactance as imaginary part can be shown within the circle of Smith chart (Fig. 17) [20].

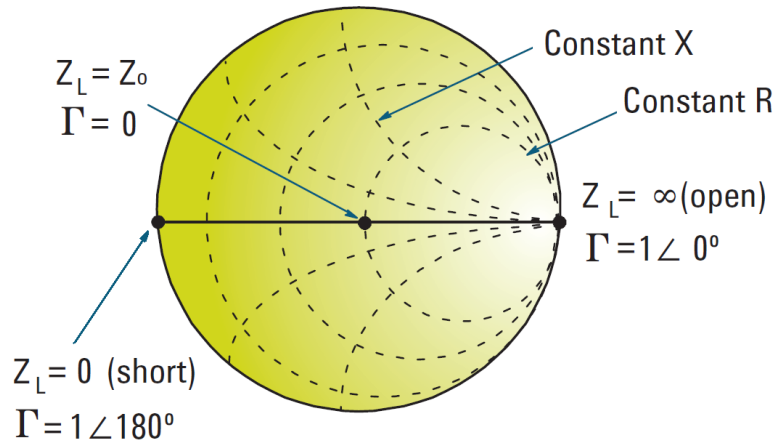








**Figure 17: Smith chart.**

### 2.4.6.3 Tools and methods

A VNA is the most important device to evaluate an RF coil. However, it is necessary, but it is not sufficient to carry out all the tests. Briefly, devices and some of their applications, which are used to evaluate the coil on the bench, are listed in Double probes or pickup loops are essentially a device to measure the  $S_{12}$  or  $S_{21}$ . It is consisted of two small single loops (usually 10 to 15 mm diameter), which are geometrically overlapped to be inductively decoupled and placed in a shield made of plexiglass. The overlapping distance can be adjusted in order to obtain a decoupling level of about  $\leq -80$  dB (in free space) between the loops. In principle, one loop induces a current in the RF coil under the test. By reciprocity, the RF coil induces a magnetic field and thus voltage in another loop. In this project, pickup loops have been often used to measure the preamplifier decoupling, tuning, transmission decoupling, and Q-factor [22, 23]. Other measurements of the coil were implemented by calibrated cables and rarely with sniffer probe (single loop).

Table 3. Double probes or pickup loops are essentially a device to measure the  $S_{12}$  or  $S_{21}$ . It is consisted of two small single loops (usually 10 to 15 mm diameter), which are geometrically overlapped to be inductively decoupled and placed in a shield made of plexiglass. The overlapping distance can be adjusted in order to obtain a decoupling level of about  $\leq -80$  dB (in free space) between the loops. In principle, one loop induces a current in the RF coil under the test. By reciprocity, the RF coil induces a magnetic field and thus voltage in another loop. In this project, pickup loops have been often used to measure the preamplifier decoupling, tuning, transmission decoupling, and Q-factor [22, 23]. Other measurements of the coil were implemented by calibrated cables and rarely with sniffer probe (single loop).

**Table 3: Useful devices and measuring tools**

Device	Category	Application	Photo
VNA	monitoring, measuring, analyzing,	coupling, decoupling, impedance, tuning, Q-factor	
Power Supply	adjustable DC Supplier	biasing preamplifiers (10V), biasing PIN Diode (100mA), rev-biasing PIN diode (-30V)	
Double Probe	measuring (via VNA)	$S_{21}$ , $S_{12}$ (tuning, isolation)	
Sniffer Probe	measuring (via VNA)	$S_{11}$ (resonance)	
Plug Interface	connector	providing scanner plugs and connections between the coil and power supply	
Coaxial Cable	connector	connecting coil or measuring tools to the VNA	



# 3 Materials and Methods

In order to start the practical phase of the project “develop an 8 channel receive-only coil for MRM at 7 Tesla”, different development aspects have been considered. As mentioned before, in order to meet the requirements, an RF coil should be exclusively designed for its specific application. For instance, in MRM, sample size is usually small. Therefore, a proper RF coil should be manufactured smaller than the other routine RF coils which are widely used for clinical scanners to study the body parts, e.g. head and neck.

In general, all the methods in previous chapter are considered as electrical aspects and to meet all of them in an ideal coil some other issues should be also taken into account during the designing. In particular, sample size and housing of the coil bring a few limitations which should be carefully treated. The following sections present the most important considerations which were met during the implementation of this project.

## 3.1 Design Considerations on Test Prototype

According to the initial definition of the project, the 8 channel receive-only coil should be integrated into the existing commercial resonator ( $^1\text{H}$  297 MHz, Rapid Biomedical, Rimpar, Germany). Furthermore, it has been investigated that the RF coil can be constructed on a flexible PCB [16]. Therefore, one of the major goals of this project was to develop the coil arrays on a flexible PCB. As a starting point for the design, first, a test loop coil was developed. Based on findings from the test prototype stage e.g. size of the coil, capacitors, and inductors, the development of the flexible PCB and coil housing were processed.

To realize the project and make it reasonable, the following steps were performed for the test loops:

- Estimating the total size of the coil.
- Estimating the size of the 8 receiver elements and arrays.
- Tuning and matching of a single element.

- Testing the transformer decoupling on an array with 4 single elements.
- Testing the overlapping of 2 single elements.
- Designing a matching network for the preamplifier decoupling.
- Testing the methods of transmission decoupling on a single element.

### 3.1.1 Coil geometry

#### 3.1.1.1 Estimating the total size of the coil

To estimate the total size of the receiver coil, first, the requirements and limitations have been reviewed. The main barrier which affected the size of the receiver coil was the size of the available resonator with inner and outer diameters of 72 and 90 mm, respectively (Fig. 18). This barrier directly defined the shape and the outer size of the receiver coil therefore it will be explained in section 3.2.1 (Coil housing) in details.

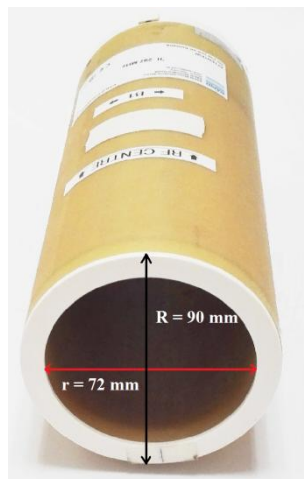


**Figure 18: Birdcage transmit coil.**

One of the requirements of this coil is that it should be able to cover a variety size of the sample containers which are different in diameter and length. Fig. 19 shows these differences. This requirement defined the inner diameter of the receiver coil.



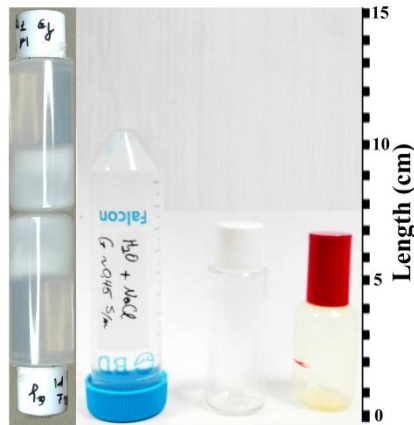


**Figure 19: Available sample containers.**

The outer diameter of the biggest sample container was about 33 mm. Therefore, to have a maximum filling factor and thus increase the sensitivity of the coil, inner diameter of the receiver coil had to be at least 34 mm. It has been reported that the highest MR signal achieves when the RF coil placed extremely close to the volume to be imaged [16].

In this step, still, estimating the total length of the coil was not possible, because it was depended on the designing of the flexible PCB and some other issues which will be discussed later.

After estimating the inner diameter of the coil housing, developing the test loop was started on a test cylinder tube.

### **3.1.1.2 Size of the test loop and array**

To determine the shape and the size of the test loop, some factors have been considered in order to increase the sensitivity of the coil. As mentioned before, ROI plays an important role to achieve a high sensitivity. On one hand, ROI is determined by the shape of the coil elements and size of the sample. On the other hand, covering the variety of samples was necessary for this coil. So the 8 receiver channels had to cover the whole length of the largest sample, which was about 115 mm. One optimizing possibility was to place the 8 channels in 2 different rows which are called arrays. Another factor to increase the ROI is the shape of each individual coil elements. Usually, four different shapes are suggested: circular, polygonal, rectangular, and elliptical [11]. In this work, to longitudinally increase the ROI with the small single loops, rectangular shape has been selected for all the single elements.

In sum, for this phase of the project, 4 individual test loops were similarly built with the following specifications:

- Material: Copper wire, 1.5 mm thick.
- Form: Rectangular.
- Size: 50 × 25 mm (L x W).

### 3.1.2 Tuning and matching

The principles of tuning and matching of the RF coils have been mentioned previously. In brief, every individual coil element must be tuned at the operating frequency or reference frequency ( $\omega_0$ ), while the output impedance of the coil is matched with the transmission lines and cables to transfer an efficient MR signal. Practically, different issues should be reviewed before a single element is tuned and matched. For instance, mutual coupling between the coil and its neighbors can change the design. A coil designer should be able to predict and to define the EMI which influence the signal and image quality.

A simple test loop is usually consisted of a loop of wire and a capacitor. Theoretically, a loop of wire, which has the inductance L, can act as a receiver antenna, when it is connected to a capacitor, C. However, in reality, this can be successfully done by trial and error.

Following steps have been done to define and design a proper test loop:

- Determining the exact operation frequency,  $\omega_0$ .
- Building the first LC test loop, finding the inductance of it.
- Finding the value of  $C_{tot}$  in which the loop resonates at the  $\omega_0$ .
- Preparing the loop for the inductive decoupling.
- Preparing the matching network.

First, the exact  $\omega_0$  was calculated by Larmor equation  $\omega = \gamma B_0$ . The exact  $B_0$  has been measured 6.98 T and the  $\gamma$  ratio for  $^1\text{H}$  is 42.58 MHz/T, so the Larmor frequency which causes hydrogen spins to precess, is exactly 297.2 MHz.

Second, a test loop was constructed in rectangular form with respect to the required size (50 × 25mm). A constant capacitor was soldered to the output of the loop. In this stage, the goal was to find out the inductance of the loop. Although theoretically, it is possible to calculate the L of the test loop, there are always some unexpected losses or other issues which change the results. Therefore, the best way to find the proper value for L is trial and error. Simply with VNA and through the pickup loops, the resonance frequency of the

LC loop can be measured. With the following equation  $\omega = 1/\sqrt{LC}$ , the inductance of the loop coil was obtained.

In third step, the target was to tune the test loop at  $\omega_0$ . By changing the value of the C and measure the frequency, the test loop was tuned to resonate at  $\omega_0$ . The final C was called C total or  $C_{tot}$ .

It has been suggested that in order to reduce the electrical length of a receiver element, the loop should be segmented by capacitors along its length. It results in reduction the radiation losses and allow a large loop to be applied at the high frequencies. Each segment should be shorter than one-tenth wavelength [6, 11].

According to the abovementioned issue and method of inductive decoupling, each single rectangular test loop was made from 1.5 mm isolated copper wire with total length of 150 mm. Since the wavelength,  $\lambda$ , of the  $\omega_0$  is around 1000 mm, so the 1/10 of  $\lambda$  is 100 mm which was shorter than the total length of the test loop. Therefore, each test loop was broken into 3 segments. Fig. 20a demonstrates a segmented test loop which was prepared for tuning and matching.

Two breaks on sides were reserved for two capacitors and two share inductors of the transformer decoupling. Share inductors are usually air core inductors which have a high Q-factor and low inductance. These inductors are made by hand. The inductance of such inductors is not only predictable with an equation but also can be measured through the VNA.

The third break which was positioned on the bottom of the test loop was considered as the output for tuning and matching capacitors and also transmission cables. Fig. 20b shows a complete test loop which can be connected to VNA for further measurements. In absence of preamplifier, a matching network can be simply one or two capacitors to match the impedance of the coil with the VNA which is 50  $\Omega$ .

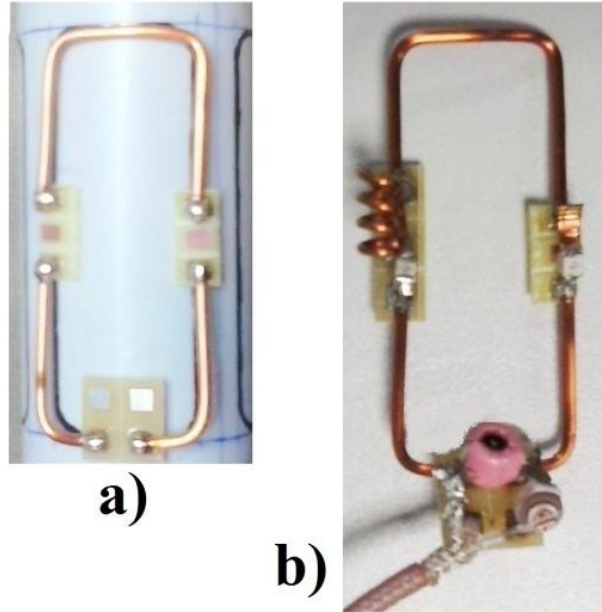


**Figure 20: Single-test loop. a) Segmented loop.**

**b) Complete test loop for resonating at the reference frequency.**

As mentioned, one important issue to increase the sensitivity of the coils is the symmetrical configuration of the elements in an array. In the test loop, the gaps on sides were connected to the tuning capacitors. To have a symmetrical geometry, the value of these capacitors had to be equal. Since the capacitors were in a series topology, the values were calculated by

$$\frac{1}{C_{tot}} = \frac{1}{C_1} + \frac{1}{C_2} + \frac{1}{C_3} \quad \text{Eq. 12}$$

where  $C_1$ ,  $C_2$ , and  $C_3$  are the tuning capacitors.

To have a fine tuning and matching, adjustable capacitors or trimmers can be applied. Inasmuch as these trimmers present a lower Q-factor than the constant capacitors, the use of them has not been recommended. Therefore, for the test loops, two trimmers were considered.

Finally, two small air core inductors with the same specifications were placed on the sides of the test loop.

During the construction of the test loop, it has been experienced that the connection between the coax cables of the VNA and the test loop is very important. It was observed that if the capacitors of the matching network were being connected on one side of the coil and not on the both sides (asymmetrical), the signal was not ideally symmetrical and

movement of the cable resulted in a noisy and unstable signal. Fig. 21 shows the difference between these two configurations.

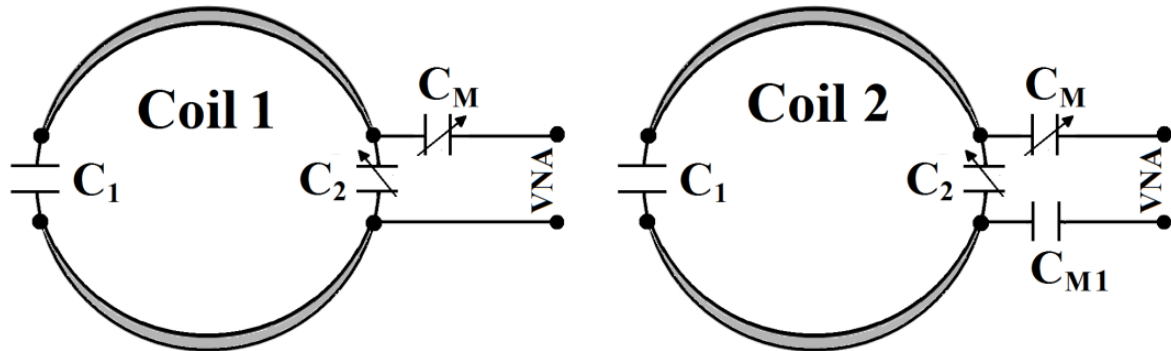


**Figure 21: Different coil configurations.**

**Asymmetrical setup (left) results in a noisy signal.**

In sum, the obtained values and parameters from previous steps were applied to build the other test channels. These values are listed as follows:

Inductance of the rectangular single loop (50 x 25 mm):  $\cong 51.2 \text{ nH}$

Tuning capacitors:

$C_1 = C_2 = 10 \text{ pF}$

$C_3 = \text{Trimmer (4.2 – 20 pF)}$

Matching network capacitors:

$C_1: 2.2 \text{ pF}$

$C_2: \text{Trimmer (1.5 – 6 pF)}$

Specifications of the air core inductors:

Wire  $\varnothing = 0.75 \text{ mm}$

Number of turns: 2

Radius of the core: 3 mm

### 3.1.3 Mutual decoupling

In this project, all the 8 channels were defined to be placed in 2 separate rows. It was predicted that the mutual coupling between the elements should be very strong since all the small elements had to be placed very close to each other. As a result, 3 different methods of decoupling have been considered as follows:

- Inductive decoupling between 4 elements in each row.
- Geometrically overlapping between the rows.
- Preamplifier decoupling for each individual coil element.

### 3.1.3.1 Transformer decoupling

Inductively decoupling is a method to isolate the channels on an array. Therefore, each test loop was equipped with 2 small inductors. Meanwhile, a remarkable issue should not be forgotten that the inductively decoupling method has the principles of overlap decoupling. Thus, if the inductors of two adjacent loops, which are located closely to each other or twisted together, would have a constructive flux density instead of a destructive, mutual coupling cannot be decreased. As a result, the flux density of one inductor should cancel out the flux density of the other one. This issue has been considered between all the loops. Fig. 22 illustrates the concept of inductively decoupling by means of twisted inductors.

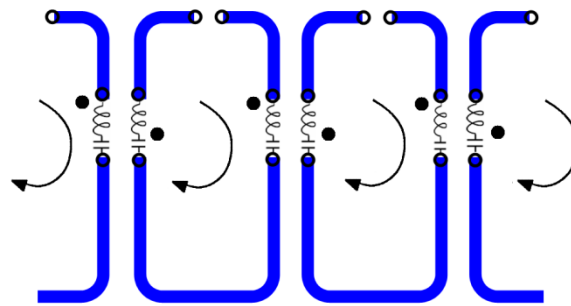


**Figure 22: Transformer decoupling between adjacent coils.**

Four test loops were placed around the cylinder and connected to the VNA through the calibrated cables. VNA is able to display not only the tuning and matching signals but also the coupling signals between the channels simultaneously.

Decoupling process has been started with changing the small inductors. For this reason, a ceramic screw was provided to open the windings of the inductors and slightly tuning them until the decoupling between the channels reached to an acceptable level.

It has been experienced that the desired decoupling level was not achievable due to the strong coupling between opposing channels, whereas they were not adjacent. Since the distance between two single loops, which are faced each other, are small ( $\sim 35$  mm), therefore, they interact with each other and cause to increase the coupling and to split the signal at  $\omega_0$ . To overcome this problem, two extra inductively networks consist of 4 small inductors and connection cables have been considered for opposing channels. Likewise adjacent channels, the Opposing channels were also shared two small inductors to reduce the coupling. Inductors were fixed on pads and placed somewhere between the channels. In this case, since the channels are not adjacent, the sharing inductors should cancel out the flux density differently. As a result, they should have constructive fields.

With the aim of reducing the EMI, the connection cables between the opposing channels and decoupling network were twisted together with the smallest possible length. Finally, after adjusting all the inductors and trimmers, tuning and matching signals with acceptable levels of decoupling were obtained (Fig. 23). This proves that the selected decoupling method is applicable for this kind of designing and can be applied for the final prototype.

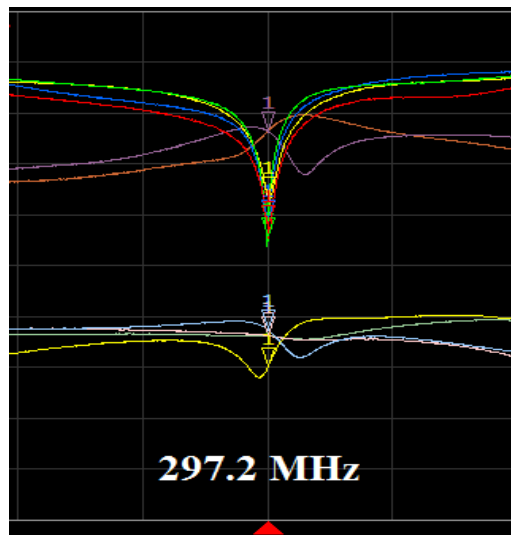


**Figure 23: Tuning and matching signals of four test loops in an array.**

### 3.1.3.2 Overlap decoupling

Geometrically overlapping should be done between two rows of the receiver coil. Although the goal of this project was to design the arrays on a flexible PCB, but to get an general overview and to have a better approximation during the PCB designing, a simple overlapping between two test loops on a flexible material was performed. The single loops were only designed to resonate at  $\omega_0$  without transformer decoupling and matching networks. Fig. 24 shows how two neighbors from different rows should be overlapped. The edge of the first single loop has to meet the center of the second test loop. The maximum isolation between two elements was achieved when they shared approximately 20% of their areas [24].



**Figure 24: Overlapping of two test loops.**

### 3.1.3.3 Preamplifier decoupling

Particularly, eight low noise preamplifiers with input impedance of  $75 \Omega$  for eight individual receiver elements have been used. It means that the best performance of the preamplifier achieves when the output impedance of the coil is set to  $75 \Omega$  [16].

The first goal of this stage was that the signal at  $\omega_0$  had to be split and the dip of the signal had to be degraded a few levels. This experiment has been done with pickup loops and through the  $S_{21}$  while the preamplifier was connected to the coil. Fig. 25 shows the goal of this step.

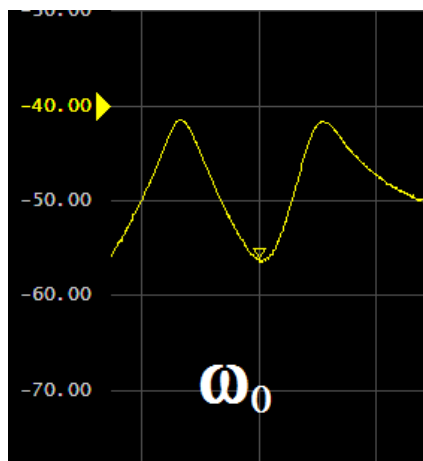


Figure 25: Decoupled signal by preamplifier.

The second goal was to measure the impedance of  $75 \Omega$  from the output of the matching network. In this step, the preamplifier had to be removed and the measurement was done with a calibrated cable and through the  $S_{11}$ . VNA was set in Smith chart. Fig. 26 illustrates the target of the measurement.

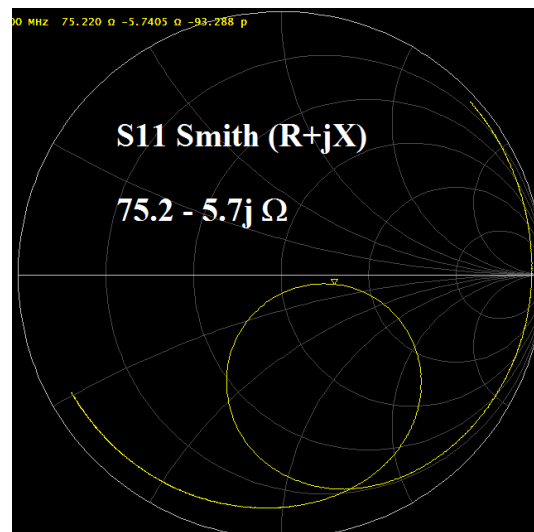
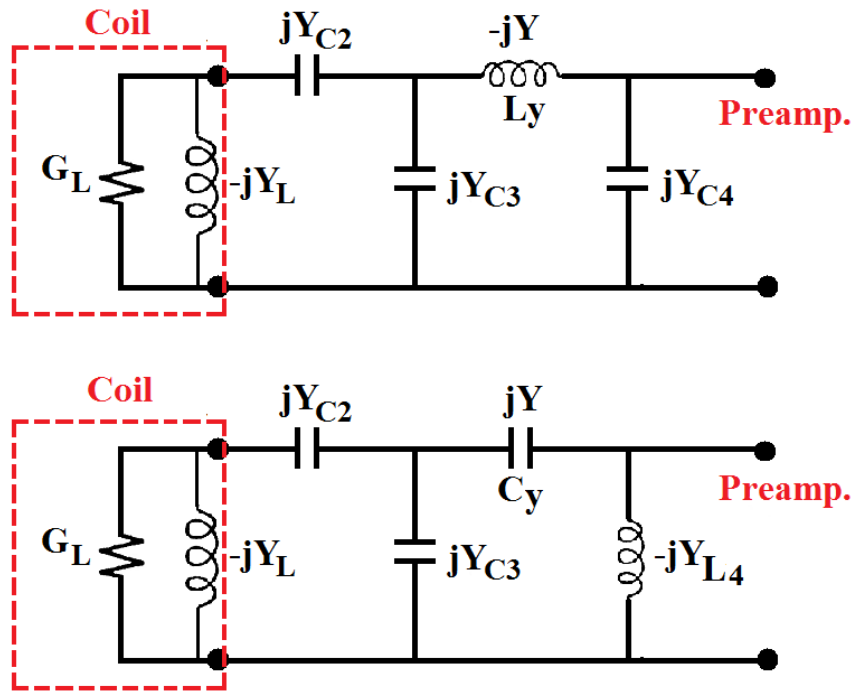


Figure 26: Matching impedance at  $75 \Omega$ .



After all, when the matching network provided the both conditions at the same time, then the coil was tuned again. In this situation, the preamplifier was removed and the input of it (output of the matching network) was closed with a  $75 \Omega$  resistor.

Since the input reflection of the preamplifier was  $0.96 \angle 40^\circ$ , so its impedance was near an open circuit. Thus, only two of the four suggested structures in the study of Reykowski et al. could be applied for the available preamplifiers (Fig. 27) [17].



**Figure 27: Possibilities of the matching network.**

One advantage of such structures is that they require only one inductor. Usually, adjusting the inductors is much more difficult than adjusting the capacitors for a high frequency.

In order to find the values of the elements in the matching network, following parameters should be known:

- Reference frequency,  $\omega_0$ ,
- Input reflection of the preamplifier,  $\phi$  (degree),
- Input impedance of the preamplifier, ( $50 \Omega$  or  $75 \Omega$ ), and
- Output impedance of the coil element,  $R_L + jX_L$ .

A set of equations were applied to find the values of the elements in the matching network [17]. Due to space restrictions, the structure at the top of Fig. 27 was selected. Moreover, in this structure, the advantage is the degree of freedom to choose the value of the inductor,  $L_y$ .

Finally, after many times trial and error, one test loop was equipped with a proper matching network with the following specifications:

$$C_2 = 33 \Omega,$$

$$C_3 = 27 \Omega,$$

$$C_4 = 10 \Omega, \text{ and}$$

$$L_y = \text{Number of turns: } 5, \text{ wire: } 0.75 \text{ mm, diameter: } 3 \text{ mm.}$$

### 3.1.4 Transmission decoupling

Two methods of transmission decoupling (active and passive) have been performed for the test loop. To implement the passive decoupling circuit, the following elements have been applied:

- Fast RF diode: 2 pcs. (Connected together inversely),
- RF Choke (1.8  $\mu\text{H}$ ): 1 pc. (Connected in parallel to the diodes to block the noise), and
- Capacitor (1 nF): 1 pc. (To block the DC current of the actively decoupling circuit).

Another option to switch between receiving and transmitting situations is to use a PIN diode. PIN diode was connected in series with L ( $L_{AD}$ ) and both were connected in parallel with C ( $C_{AD}$ ). The parallel configuration of  $L_{AD}C_{AD}$  was tuned at  $\omega_0$ . Hence its resonating caused an interference with the receiver coil which was also tuned at  $\omega_0$ . As a result of strong coupling between receiver coil and  $L_{AD}C_{AD}$ , the signal of the receiver coil was split at  $\omega_0$ , causing the isolation of the receiver coil from the transmitter [24].

Usually, the PIN diode is connected to the DC bias through the RF chokes. These chokes present a very high impedance at  $\omega_0$ , but during the transmission phase, they pass the DC current to feed the PIN diode. At the same time, to isolate the DC lines from each other, a capacitor can be used between the ground and bias. The reason, which causes the RF chokes and capacitors behave differently, is the frequency [11]. The impedance of the capacitors and inductors depends on the frequency by

$$\text{At high frequency} \rightarrow |Z_c| = \frac{1}{j\omega C} \cong 0 \equiv \text{short circuit,}$$

$$|Z_L| = j\omega L \cong \infty \equiv \text{open circuit}$$

$$\text{At low frequency (DC)} \rightarrow |Z_c| = \frac{1}{j\omega C} \cong \infty \equiv \text{open circuit,}$$

$$|Z_L| = j\omega L \cong 0 \equiv \text{short circuit}$$

Measuring the function of the actively decoupling is possible with VNA, power supply, pickup loops and through the  $S_{21}$ . The following elements were applied to the circuitry of the active detuning:

PIN diode: 1 pc.

RF Choke (1.8  $\mu\text{H}$ ): 2 pcs.

Capacitor (1 nF): 1 pc.

$L_{AD}$ : Number of turns: 3, wire: 0.75 mm, diameter: 4 mm

$C_{AD}$ : 4.7 pF

The point is that the circuitry of the passive detuning uses also the  $L_{AD}$  and  $C_{AD}$  for the transmission decoupling. Fig. 28 illustrates the circuitries of the passive and the active decoupling.

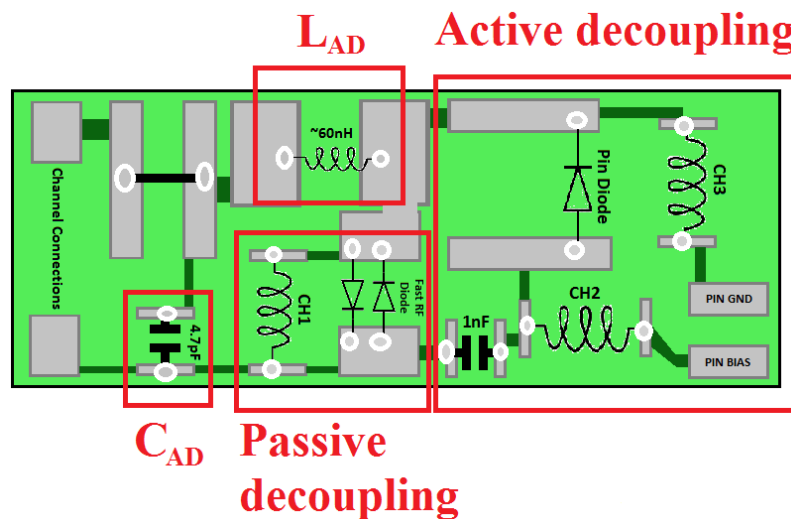


Figure 28: Different circuit diagrams of transmission decoupling.

## 3.2 8-channel Coil Array Construction

### 3.2.1 Coil housing

Conceptually, the housing of the receiver coil was defined as a proper structure for placing the electronic circuitries, components, and cabling. The structure must be fitted inside a special transmitter coil and different types of sample containers as illustrated in Fig. 19 must be covered by the coil. All the requirements and limitation for the housing of the receiver coil are listed in Table 4 [27].

**Table 4: Requirements and limitations of the coil housing**

Requirement	Limitation for Receiver Coil
Transmitter fitting	diameter of the outer cylinder $R \leq 71.5 \text{ mm}$
Sample compatibility	diameter of the inner cylinder $r \geq 34 \text{ mm}$
Scanner cable connection	required diameter = 17 mm
MR compatibility	materials with low dielectric constant
Circuitry and components	min. distance between inner and outer cylinder $(R - r)/2 \geq 16 \text{ mm}$
Long sample compatibility	open ended design

According to the first description of the housing, the following steps have been done:

- The first design was created on the paper and its function, advantages, and drawbacks were discussed with specialists. After revising the first design, the shape and the required parts of the housing were defined as follows:  
 “The housing of the 8 channel receive-only coil should be designed cylindrical to be placed within the transmitter coil. Its material should have a very low loss tangent. Loss angle describes dielectric losses of a specific material. This value is inversely proportional to the Q-factor. Therefore, high Q-factor increases when the  $\tan \delta$  becomes small [16]. The housing can be consisted of 4 parts; inner cylinder, outer cylinder, front side cover and back side cover. Scanner cable should be connected to the back side cover. The back side cover should be opened for long sample containers. Center of the receiver elements should be located at the  $B_1^+$  center of the transmitter coil (Fig. 29).
- The inner and outer cylinders have been ordered by a company which offered phenolic paper with the loss tangent of about 0.04. Usually, the bodies of the coils are made from phenolic paper, glass fiber or Teflon [25].
- Designing the front and back side covers were performed in a 3D CAD (Computer-aided design) software. During the drawing, 3 different holes on each side cover have been considered for fixing the cylinders into the side covers.

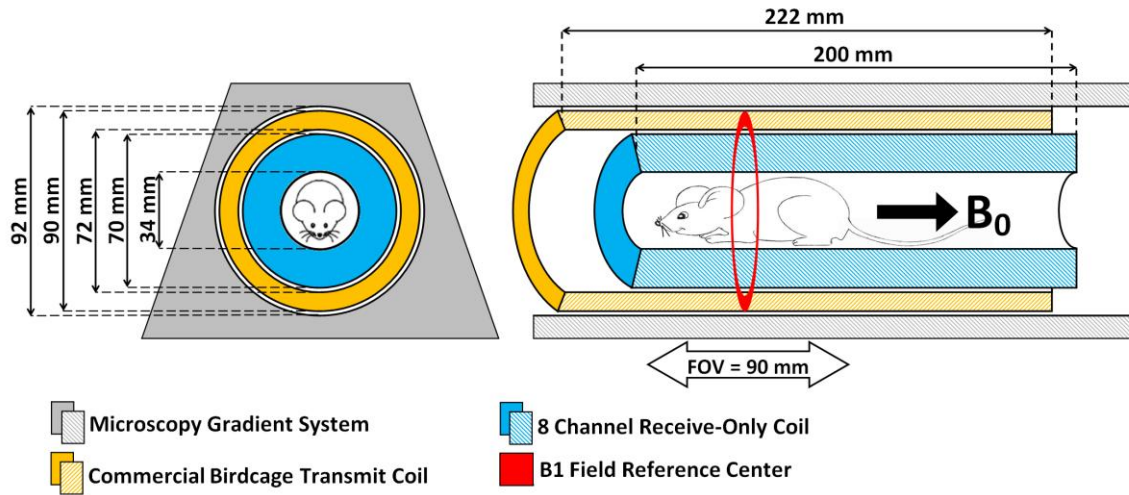


**Figure 29: Estimating the size and the shape of the coil.**

Due to the complex geometry of the side covers, these components were ordered to be constructed by 3D printers and to be made from Teflon.

After all, when the side covers were delivered, the complete housing was tested without any circuitry and cabling for final adjustments or if necessary post treatments.

Precise dimensions and specifications of the coil housing which consists of 4 different components are listed below:

- Inner cylinder (Fig. 30a)
  - Outer diameter,  $D$ :  $36 \pm 0.1$  mm
  - Inner diameter,  $d$ :  $34 \pm 0.1$  mm
  - Wall thickness:  $1 \pm 0.1$  mm
  - Length:  $190 \pm 1$  mm
  - Material: phenolic paper (loss tangent: 0.04)
  - Color: brown
- Outer cylinder (Fig. 30b)
  - Outer diameter,  $D$ :  $71 \pm 0.2$  mm
  - Inner diameter,  $d$ :  $68 \pm 0.2$  mm
  - Wall thickness:  $1.5 \pm 0.2$  mm
  - Length:  $200 \pm 1$  mm
  - Material: phenolic paper (loss tangent 0.04)
  - Color: brown
- Front side cover (Fig. 30c)
  - Inner diameter,  $d$ :  $34 \pm 0.1$  mm

Outer diameter, D:  $71 \pm 0.1$  mm

Length: Max.  $7 \pm 0.1$  mm

Material: Teflon

Color: white

- Back side cover (Fig. 30d)

Inner diameter, d:  $34 \pm 0.1$  mm

Outer diameter (inside), D:  $71 \pm 0.1$  mm

Outer diameter (outside), D:  $90 \pm 0.1$  mm

Length: Max.  $25 \pm 0.1$  mm

Material: Teflon

Color: white

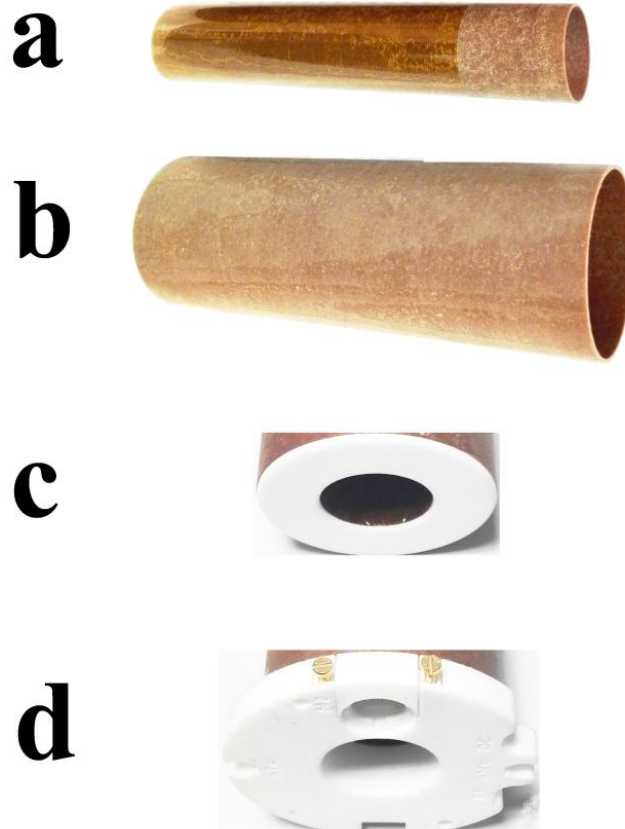


**Figure 30: Components of the coil housing. a) Inner cylinder.**

**b) Outer cylinder. c) Front side cover. d) Back side cover.**

### **3.2.2 PCB design**

With the purpose of bending the channels around a cylindrical tube, the circuitry and channels were designed and printed on a flexible PCB. For microscopy purposes, the space is very critical. It has been suggested that the construction of the coil elements can be done with using the flexible circuit boards. Usually, copper is coated within a material made of polymer e.g. PTFE or polyimide. In order to use such materials for PCB, the loss angle or  $\tan \delta$  of the material should be as low as possible [16].

To design the PCB, a workflow has been performed:

#### **3.2.2.1 PCB manufacturer and material**

To have a suitable design, first, a manufacturer that was capable to produce the flexible PCB has been found.

Usually, manufacturers offer similar materials for a same technology. Differences can be in delivery time, the minimum and maximum size of the board, and the cost of the board per square cm. For this project, the manufacturer had to be able to produce the double layer flexible boards. On the other hand, the using material had to have a very small loss angle.

A double layer PCB gives the advantage of having separate planes to design the circuitry, thus, saving the space. For this project, a double layer PCB was very convenient, because all the receiver channels were printed on the 1<sup>st</sup> layer and the whole circuitry was printed on the 2<sup>nd</sup> layer.

A double layer flexible PCB with a proper material made of polyamide, which has a dielectric constant of about 3.6 and loss angle of about 0.008, has been ordered [26, 27].

#### **3.2.2.2 PCB specifications**

General properties, technical specifications and limitations of the PCB are very important. Knowing these information helps to protect the PCB and to modify the designing. In particular, the stability of the solder pads under temperature is one of the general specifications. Selecting a proper solder and soldering iron, which work properly at that specific temperature, ensure the function of the PCB. It has been mentioned that the copper adhesion degrades significantly with increasing the temperature [27].

PCB designing usually suffers from technical specifications of the PCB. This information must be considered during the drawing which can limit the design. Major specifications of the flexible PCB are minimum and maximum size of the circuit board, minimum size

of the conductor width, minimum diameter size of the vias, and minimum distance between two traces,. Vias are the holes to connect the conductors of different layers. Fig. 31 shows the structure of the used double layer flexible PCB in this project.

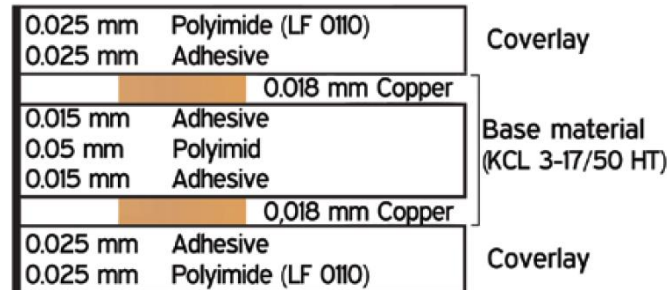


**Figure 31: Structure of the two layer flexible PCB.**

### 3.2.2.3 Schematic circuitry of the coil

Like any other electronic circuitry, a receiver coil needs also a schematic design to describe the connections between the elements. This diagram can be used to produce the PCB. For this purpose, a special software package which is called Proteus (Version 8.0, Labcenter electronics Ltd., North Yorkshire, England) was applied.

Proteus is a powerful working environment to generate schematic captures and to develop PCB. To implement the electronic circuitry of the receiver coil with the software, following steps have been done:

- Designing a single loop with associated segments, saving it as a new package.
- Designing a preamplifier according to the available preamplifier, saving the drawing as a new package.
- Designing a complete single channel receiver coil with all necessary packages and elements, e.g. sockets, ground and bias units.
- Customizing all the labels and values of the elements according to previous finding and datasheets.

One important issue in this stage was that due to the similarity and symmetry between arrays, only one complete receiver channel has been drawn. This complete channel was later used to develop the PCB. Fig. 32 demonstrates the circuit diagram of a complete single channel in the receiver coil.



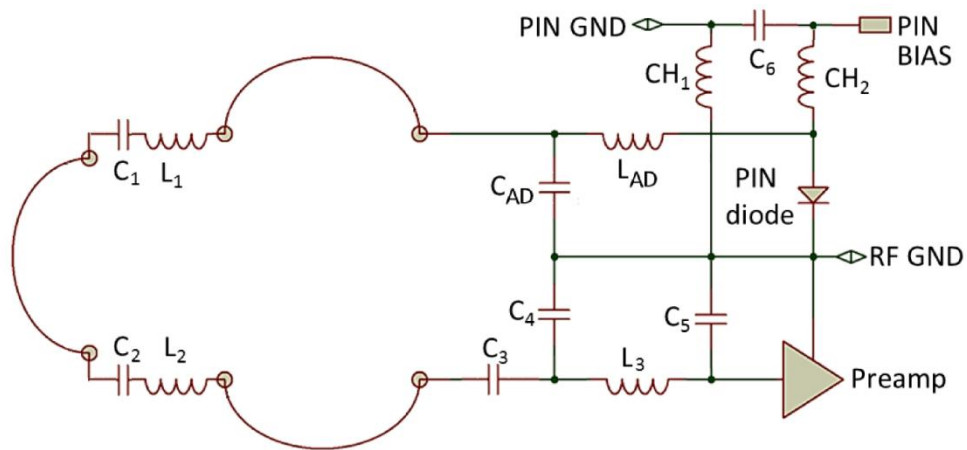


**Figure 32: Schematic circuit diagram of a single channel.**

### 3.2.2.4 PCB drawing

A printed circuit board is a board to support the circuitry electronically and mechanically. It provides the routes for signaling between the elements and also supports the components to attach physically to the board through the pads. The material of pads and routes must be very conductive. Instead, the material of the substrate, which includes the routes and pads, must be very non-conductive. For the used flexible PCB, this substrate had a dielectric constant of about 3.6.

In order to have a good PCB layout, a lot of recommendations and considerations should be applied which are beyond the topic of this project. However, some major issues to design the PCB can be mentioned briefly.

Before starting to design the PCB, it would be useful to see the other designs as an example. One feature is the Help option of the PCB environment which includes the most of the requirements and descriptions of elements. Realizing the component placement is very important. This can be happened on a piece of paper or in a computer, but it is very necessary to do it before designing the PCB. The layout recommendations of the PCB must be reviewed to adjust the setting of the software (Table 5). Another issue which should take into account is to use the schematic for drawing the PCB. Although using only the PCB environment without schematic is a feature, but using the schematic diagram to design the PCB ensures that the components are correctly connected together. It also helps to have a simple component replacement.

**Table 5: Specifications of the flexible PCB**

Technical Parameters (flexible PCB)	
Max. size of the circuit board	Length: 400 mm Width: 250 mm
Min. size of the circuit board	Length: 10 mm Width: 35 mm
Min. conductor width, conductor clearance	150 $\mu\text{m}$
Vias	via diameter $\geq 300 \mu\text{m}$
Min. via-via spacing	450 $\mu\text{m}$
Min. milling radius	500 $\mu\text{m}$
Min. copper-contour clearance	300 $\mu\text{m}$

To get a higher image quality, the location of the preamplifiers is very important. It has been suggested that the preamplifiers must be located as close as possible to the coil elements. Therefore, the MR signal passes the shortest way between the antenna and the preamplifier [28]. Accordingly, the placement of the matching network which is between the channel output and the preamplifier becomes important. As a practical experience, in section 3.1.3.3., the only difference between the two suggested structures for the matching network (Fig. 27) was the location of  $C_4$  and  $L_y$ . During the PCB designing, due to the small available space, this capacitor,  $C_4$ , was placed under the empty space of the preamplifier. However, this was difficult for the  $L_y$ .

In a schematic diagram, the locations of the components are not cared because there is enough space to put the elements everywhere. Whereas the most important issue in PCB designing is the orientation and placement of the components.

After designing the schematic diagram of a single channel receiver coil, PCB designing of the 8 channel receiver coil was started. Since there were two rows of arrays, which had to be overlapped, the design of the PCB was done individually for both rows. The first row included the receiver elements of 1 to 4 and the second row included the receiver elements of 5 to 8. Practically, following considerations have been treated:

- All the 8 antennas, associated circuitries, pads and vias were implemented on a 0.2 mm double layers flexible PCB.
- All the receiver antennas were printed on the 1<sup>st</sup> layer and connected through the vias to their circuitries on the 2<sup>nd</sup> layer.
- The width of the each trace of the antenna was 2 mm and the minimum distance between two traces of adjacent antenna, which carry the MR signal, was 4 mm. This decreases the chance of the cross talk and therefore reducing the EMI.
- Every single antenna consisted of 3 segments that were connected to the 2<sup>nd</sup> layer through the vias.
- Geometry and size of the all 8 antennas were equal to each other.
- To ensure that the impedance is continuous across the bends in antenna elements, a 45° bend trace instead of a right angle bend trace was considered for the routes.
- Symmetric configuration of the antenna traces was considered for all the 8 channels. However, due to the limitations in sample positioning and not enough space in the housing, a symmetric configuration has not been applied for the circuitries on two different rows. It was only considered for the channels which were located in a same row.
- For all the channels, DC ground was shared with the matching network and input of the preamplifier.
- For all channels, matching networks and preamplifiers were placed as close as possible to the output of the antenna traces.

Fig. 33 demonstrates the final PCB design of the 8 channel receiver coil. The blue traces are the receiver channels and the red areas are the location of pads and circuitry.

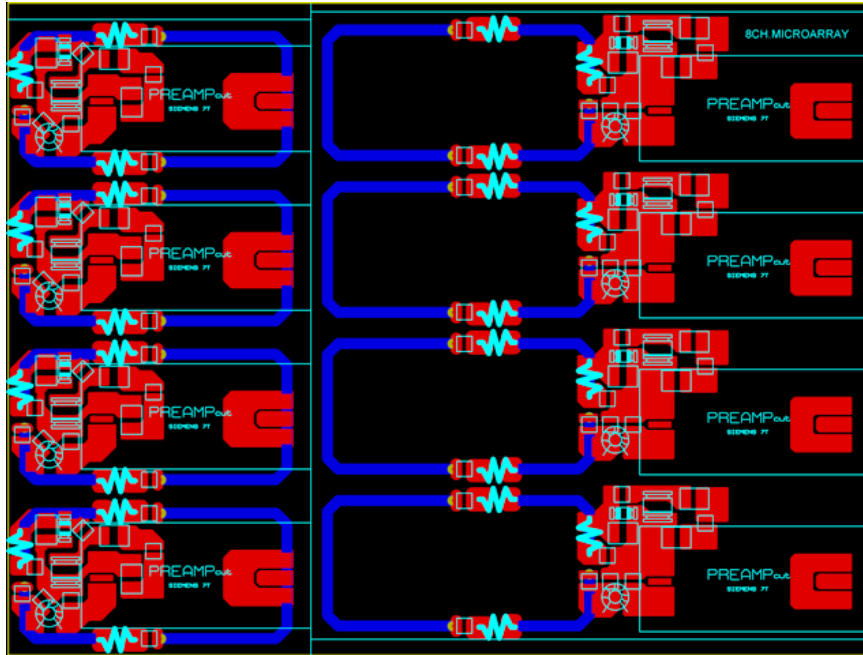


**Figure 33: Schematic of the PCB of the receiver coil.**

To find the design problems, printing the final design on a sheet of paper and testing the design on the housing can be very helpful. Therefore, it has been done carefully in this work to ensure whether the size of the board covers the cylinder tube.

Finally, before ordering the PCB, all the connections, traces, and layers were checked again. Settings of the software were controlled and the unnecessary writings, labels, and values were removed or hidden. To reduce the cost of the ordering, two different designs were printed on a one single PCB. The flexible PCB was ordered at PCBPool (Beta LAYOUT GmbH, Aarbergen, Germany).

### 3.2.3 Coil construction

#### 3.2.3.1 PCB preparation

Before starting to solder the components on the PCB, all the pads, connections, traces and vias were exactly tested. Since the antenna traces are coated on the PCB, it was important to check them optically and technically.

All the 8 channels and associated circuitries were printed on a single sheet flexible PCB, therefore, it was necessary to separate the 1<sup>st</sup> and 2<sup>nd</sup> rows from each other (Fig. 34a). This was done by cutting the PCB from its board edges which were printed on it. After that, both arrays were wrapped around the inner cylinder of the housing to check the size. Accordingly, a small difference between the circumferences of the inner cylinder and the

wrapped arrays has been found. This difference was about 3 mm which caused the arrays were loosely placed around the cylinder.

This difference in circumferences was also calculated in this way:

- Housing: Outer diameter of the cylinder,  $D$ : 36 mm  $\rightarrow$  Circumference,  $C_{\text{cylinder}} = \pi \cdot D = 3.14 \times 36 \cong 113 \text{ mm}$
- PCB array: width of an antenna = 25 mm, distance between two adjacent antennas: 4 mm  $\rightarrow$  Circumference of the warped PCB array,  $C_{\text{PCB}} = (4 \times 25) + (4 \times 4) = 116 \text{ mm}$
- $C_{\text{cylinder}} - C_{\text{PCB}} = 113 - 116 = -3 \text{ mm}$

Negative value means that the cylinder housing should be thicker. To solve the problem, a special kind of adhesive tape called Kapton® was applied to make the circumference of the cylinder thicker. Kapton® is usually made from polyimide film and a layer of adhesive silicon which possess a very good resistance against temperature and also a very low loss tangent. Therefore, the inner cylinder of the housing was coated with a layer of Kapton®. In addition, as the Kapton® can be easily cleaned, the inside surface of the inner cylinder, where the sample must be located, was also coated with Kapton®.

Finally, flexible PCBs of the 1<sup>st</sup> and 2<sup>nd</sup> arrays were wrapped around the inner cylinder and the sides of each PCB were glued together (Fig. 34b).

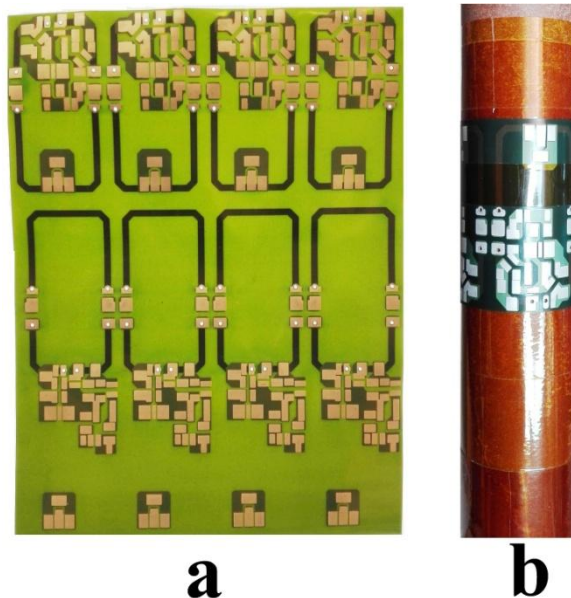


**Figure 34: Flexible PCB arrays. a) Channels and circuitries are printed on two different layers. b) A wrapped array around the coated housing.**

### 3.2.3.2 Single channel development

After PCB preparation, all the channels were numbered from 1 to 8. Channels 1 to 4 (CH1, CH2, CH3, CH4) on the 1<sup>st</sup> row and channels 5 to 8 (CH5, CH6, CH7, CH8) on the 2<sup>nd</sup> row were labeled. Thereafter, CH1 and CH5 were selected from different arrays for the first development process. The first stage was to implement the tuning and matching components. However, the size and cross section of the antenna on the PCB were similar to the test prototype, but it has been experienced that the values of the elements had to be modified for the printed antenna. Therefore, with trial and error some new values were found for CH1 and CH5. Furthermore, other circuitry blocks were completed for CH1 and CH5, e.g. transmission decoupling and matching network. S-parameter methods were performed to evaluate the impedance and resonance. In this stage, two arrays were located far from each other without any overlapping to reduce the EMI. Overlapping has been done when all the 8 channels were completely developed. In order to measure the correct responses from the channels, during the development, a sample was always inserted inside the housing.

### 3.2.3.3 Array development

All the other channels (CH2, CH3, CH4 from the 1<sup>st</sup> array and CH6, CH7, CH8 from the 2<sup>nd</sup> array) were constructed similarly to the CH1 and CH5.

To reduce the mutual coupling between the adjacent channels, transformer decoupling was performed. Meanwhile, measuring the coupling between opposing channels by means of preamplifier decoupling instead of transformer decoupling was investigated. In fact, if the test had an acceptable level of isolation at  $\omega_0$  without any splitting, the inductors of the transformer decoupling for the opposing channels could be removed.

To perform the test, a preamplifier was connected to CH1 and the  $S_{11}$  of the CH3 which is faced to CH1 was monitored. Also, all the other channels were decoupled during the test. It was observed that EMI affects the signal, meaning that isolation was not enough (Fig. 35). Therefore, transformer decoupling was applied not only for the adjacent channels but also for the opposing channels.

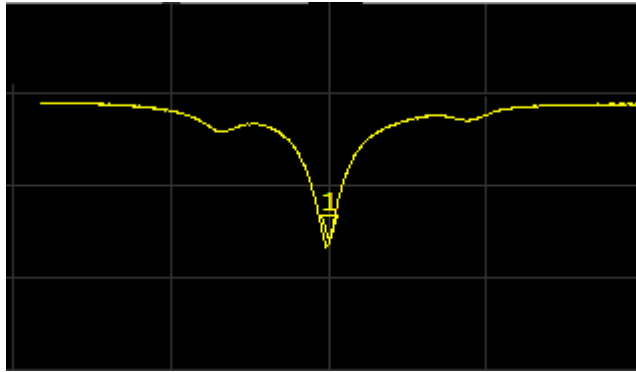


**Figure 35: Channel isolation only by preamplifier decoupling.**

Despite adjusting, plugging and unplugging the preamplifier had to be done very carefully. The small sockets of the preamplifier were connected on the curved PCB which could break every time that the impedance matching or preamplifier decoupling was being investigated. This can be seen in Fig. 36. The solder pad on the PCB became damaged and had to be replaced with a piece of copper foil.



**Figure 36: Removing the solder pad from the PCB.**

Finally, when the both arrays with 8 channels were constructed, an S-matrix was prepared to evaluate the coupling levels between the channels on each row. 6 measurements for the 1<sup>st</sup> row and 6 measurements for the 2<sup>nd</sup> row were performed.

Row 1:  $S_{12}$ ,  $S_{13}$ ,  $S_{14}$ ,  $S_{23}$ ,  $S_{24}$ ,  $S_{34}$

Row 2:  $S_{56}$ ,  $S_{57}$ ,  $S_{58}$ ,  $S_{67}$ ,  $S_{68}$ ,  $S_{78}$

### 3.2.3.4 Overlapping

This step was done, when the both arrays were completely constructed. The important point was that the orientation of the channels in different rows had to be fixed during the overlapping process. It means that channels from opposing rows must have  $45^\circ$  differences during the overlapping. In other words, the edges of two adjacent antennas must be placed at the center of the channel which locates on the opposing row (Fig. 37). Overlapping has been done under the abovementioned condition. The rows were only moved in longitudinal axis. The suitable distance, where the minimum coupling between the rows can be obtained, was found by trial and error.

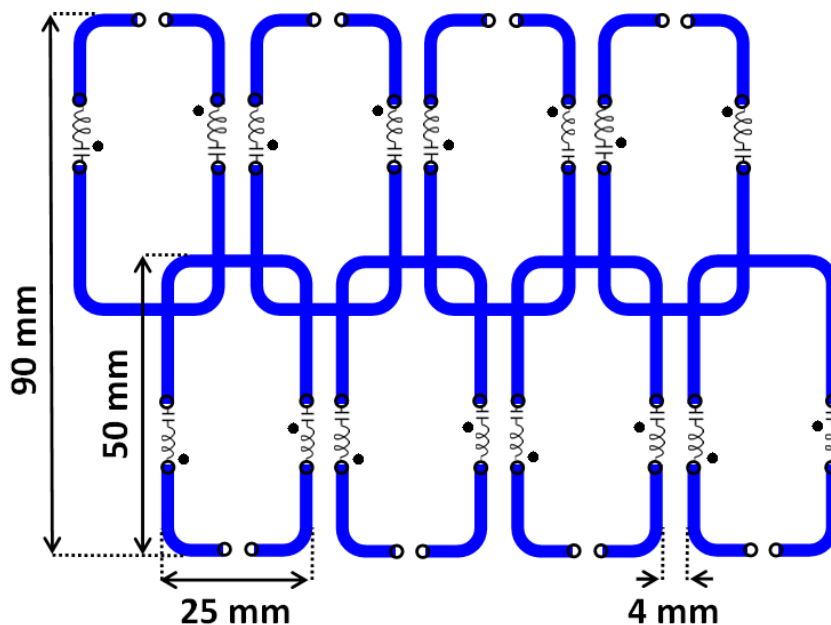


Figure 37: Final location of the arrays after overlapping.

One interesting issue in this test was that two typical channels from two different rows, which faced each other, interacting significantly together. Therefore, overlapping process was done while the  $S_{12}$  monitored the coupling levels of such channels.

### 3.2.3.5 Optimizing the channels

After all modifications and changes, at the final stage, tuning and matching were performed again for all the channels. The overlapping process changed some parameters, thus retuning the channels and adjusting the impedances had to be done once more.

It has been experienced that the capacitor,  $C_2$ , from the matching network has a critical role. This capacitor could adjust the impedance matching while changing the tuning and



vice versa. Therefore, a trimmer instead of a constant capacitor was placed in order to have a fine adjusting between matching and tuning.

Furthermore, air core inductors, which have a very high Q, were applied for all of the channels. The drawback of such an inductor is its sensibility to movements. Therefore, all the inductors were glued and fixed with epoxy which has a very low loss tangent and a good transparency in MRI.

The final components and their values for both arrays are listed in Table 6.

**Table 6: List of the applied elements for the 8 channel receiver coil**

	Row 1	Row 2
Component	CH1 - CH4	CH5 - CH8
$C_{TUNE}$	5.6 pF	5.6 pF
$C_{TUNE}$	7.5 pF	7.5 pF
$L_{DECOUPLING}$	2 T, 0.75 W, 3 Ø	2 T, 0.75 W, 3 Ø
$C_{2, MN}$	Trimmer (1.6 - 4 pF)	Trimmer (1.6 - 4 pF)
$C_{3, MN}$	51 pF	59 pF
$C_{4, MN}$	20 pF	23 pF
$L_{y, MN}$	3 T, 0.75 W, 2.9 Ø	3 T, 0.75 W, 2.9 Ø
$L_{AD}$	4 T, 1.0 W, 4.0 Ø	4 T, 1.0 W, 4.0 Ø
$C_{AD}$	4.7 pF	4.7 pF
RF CHOKE	1.8 µH	1.8 µH
Diode	PIN	PIN
Preamplifier	Siemens 7T, 75 Ω	Siemens 7T, 75 Ω

## **3.2.4 Interfacing to the MR scanner**

### **3.2.4.1 Scanner cable connection**

Every scanner has its own cables and interfaces. Accordingly, for this coil, a special kind of multi conductor cable which is compatible with 7T Siemens scanner was used. This cable has two sides and consists of DC, signal and ground cables. Also, each cable can support up to 8 receive channels. Connector which must be plugged into the scanner is located on one side. The other side is free for single cables which should be modified for each individual channel.

Main cable was fixed to the back side cover of the coil and each individual cable was connected to the proper channel. The point is that the DC and signal cables have different colors to easy identifying and tracking. Therefore, each cable, which had a number from 1 to 8, was connected to the corresponding channel.

In order to achieve the highest distance between cables and circuitry, which can reduce the EMI, a holding structure made of plexiglass was built to fix the cables and thus keep the distance as far as possible (Fig. 38).

Another important point is that each coil must take an identification number which is exclusively defined for each coil. This helps the scanner to recognize the different coils when they are plugged. Identification number is called coil code. Coil code should not be occupied with another coil. In order to specify a code (a two-digit number) to the receiver coil, first, the exclusive code has been written in the main computer of the scanner. Second, the code was made with special kind of resistors and was connected inside the cable connector. Without identification number, the scanner cannot recognize and accept the coil.

### **3.2.4.2 Cable trap**

One very important point in both receiver and transmitter coils is the common mode current or shield currents. Specifically, in phased array coils, it degrades the isolation between the channels and affects the performance of the coil. When the shield currents are produced on the coaxial cables, they can change the tuning and matching of the coil, therefore their effects must be removed. A cable trap is usually an LC circuit which resonates at  $\omega_0$ . Consequently, two types of cable traps were applied in this work [29].

- Floating cable trap, and
- Wound coaxial cable trap.

Type one was used before the first MR experiment and type two was additionally connected after the MR experiment. The reason was to improve the  $B_1^+$  homogeneity. One floating cable trap has been built to resonate at  $\omega_0$ . Then it was fixed around the scanner cable and near the receiver coil. This type of trap does not need to be physically connected to the transmission line. Conversely, the second type of the traps must be connected physically to each coaxial cable. The best place for them is inside the coil and slightly after output of the preamplifiers. They can be made small enough to be placed in microscopy coils. Therefore 8 single cable traps were made with toroidal inductors to resonate at  $\omega_0$  (Fig. 38).

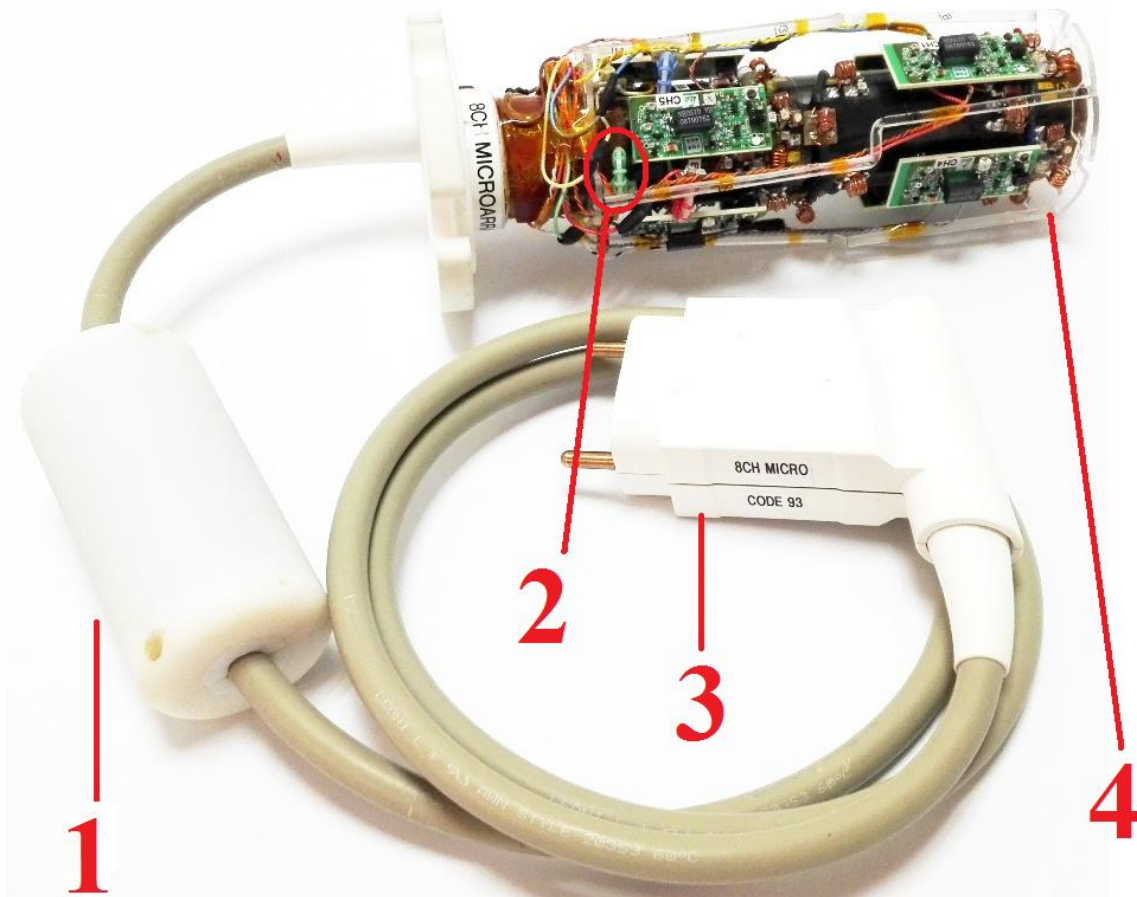


**Figure 38: Different parts of the final receiver coil. 1) Floating cable trap. 2) Wound coaxial cable trap. 3) Scanner connector. 4) Cable holding structure.**

### 3.2.4.3 Transmit coil adjustment

Since the receiver coil is placed inside the transmitter, it affects the tuning and matching of the transmit coil. The commercial transmit coil can be tuned and matched from outside through remote variable capacitors. Therefore, after loading the sample inside the receiver, transmit coil must be adjusted again. For this purpose, the sample and the receiver were placed inside the transmitter. Both transmitter and receiver were connected to the proper interfaces in the lab and the output signal of the transmitter was connected to the analyzer. Then, the transmitter was tuned and matched while the receiver was decoupled or to be precise when the PIN diodes of the 8 channels were biased forward. Fig. 39 and Fig. 40 demonstrate the final view of the receiver coil alone and in combination with transmitter coil.



**Figure 39: Complete view of the 8 channel receive-only coil.**

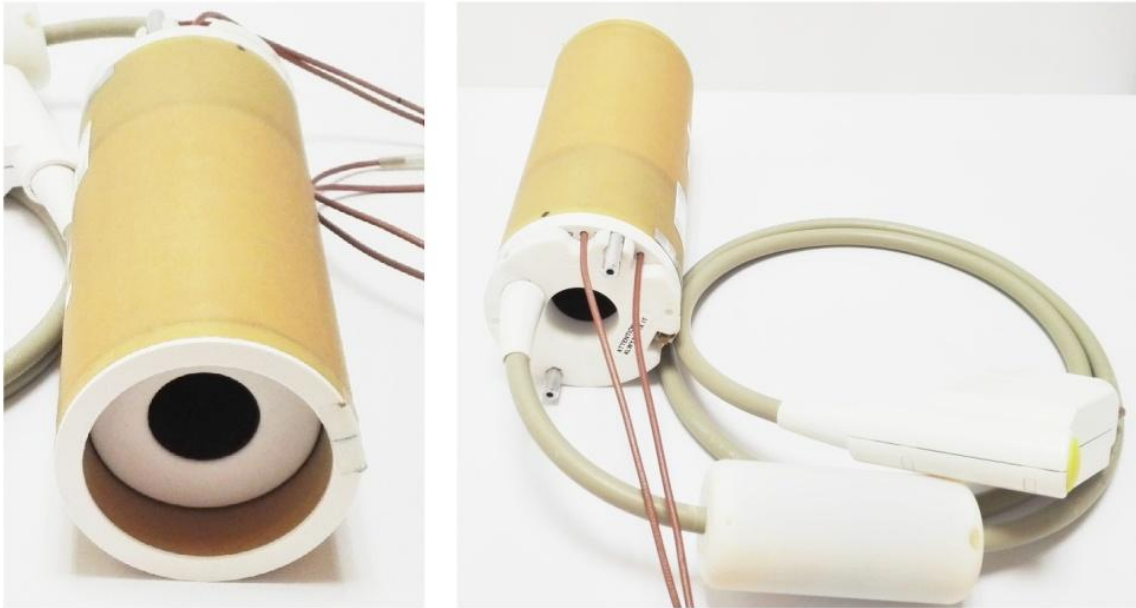


**Figure 40: Front side and back side views of transmit and receive coils.**

### **3.3 Performance Testing**

#### **3.3.1 Bench tests**

In each step of the development, different parameters of the coil elements such as tuning and matching, isolation, and decoupling should be evaluated in order to be sure about the correct performance of the coil. These types of evaluations are called workbench measurements and presented a very good evaluation of the function of the RF coil.

##### **3.3.1.1 Tuning and matching**

Tuning and matching the channels were done through the  $S_{12}$  and  $S_{11}$ , respectively. Pickup loops measured the tuning and a calibrated cable monitored the impedance on Smith chart. Tuning and matching are correlative processes. In the same way, every change in the circuit e.g. adding the cable traps results in changing the tuning and matching impedance. The only variable capacitor,  $C_{2\text{ MN}}$ , of each channel was placed at the output of the antenna and input of the matching network. So, tuning and matching were adjusted by screwing the  $C_{2\text{ MN}}$ .

### 3.3.1.2 Inter-element decoupling

Mutual coupling between the elements in an array should be measured. Usually, coupling between the receiver elements split the signal at  $\omega_0$ , thus the coil cannot detect the MR signal. Evaluation was done not only for the 8 channels on the PCB but also for the 4 channels on test prototype. Measurement was performed through the  $S_{12}$  and with two different calibrated cables which were equipped with several ferrites in different places of the cable to reduce the EMI.

To evaluate the results, a matrix which is called scattering matrix (S-matrix) has been prepared. Since there are 4 channels, a  $4 \times 4$  matrix was needed. The reason was that every single element had to be isolated from other 3 channels which increased the number of measurements. Values of  $S_{ij}$  presented the isolation level in dB. An important issue in S-matrix of the mutual coupling is that the  $S_{ij}$  is equal to  $S_{ji}$ , which builds a symmetric matrix. Therefore, the half of the matrix which is occupied by the same numbers can be removed. A typical matrix for a 4 channel receiver coil is as follows:

$$S_{ij} = \begin{pmatrix} S_{11} & \cdots & S_{14} \\ \vdots & \ddots & \vdots \\ S_{41} & \cdots & S_{44} \end{pmatrix} \quad \text{Eq. 13}$$

### 3.3.1.3 Transmission decoupling

In order to evaluate the active detuning, preamplifiers must be unplugged and replaced with  $75 \Omega$  resistors. Pickup loops measured the  $S_{21}$  between the tuning and detuning situations. For this purpose, when one channel was under the test, the other 7 channels had been detuned through their PIN diodes. During detuning, if the dip of the signal was not at the  $\omega_0$ , with adjusting the  $L_{AD}$  (opening or closing), the dip was shifted to the right or left position where the  $\omega_0$  located. Another important point in active decoupling was the distance between two decoupled peaks. Usually, when the LC trap ( $L_{AD}C_{AD}$ ) operates properly, then the peaks are located symmetrically and dip will be place at  $\omega_0$ .

### 3.3.1.4 Q-factors

Different studies suggested similar methods to estimate the resistive losses of the sample and coil. For this reason, a receiver channel tuned at  $\omega_0$  should be tested in 2 different situations, with sample (loaded) and without sample (unloaded). These situations are called,  $Q_{load}$  and  $Q_{unload}$  or briefly,  $Q_L$  and  $Q_U$ . The ratio of these parameters indicates that

if the sample noise is not dominance then increasing of SNR can be expected. In general, a coil with  $Q_{ratio}$  below 2 is not a good coil [10]. This can be achieved by

$$Q_{ratio} = \frac{Q_U}{Q_L} \quad \text{Eq. 14}$$

One of the reasons to measure the Q-factor is to select the proper material and to find the optimized size and geometry for the loops. Since the design choices in this project were limited and the target was to focus on flexible PCB, the  $Q_{ratio}$  of the test prototype was measured one time to ensure that the selected size and geometry presented enough efficiency. Through the VNA and measuring the  $S_{12}$ , this ratio has been calculated.

The only difference between  $Q_L$  and  $Q_U$  is the presence of the sample. Q for both situations can be calculated by

$$Q = f / \Delta f \quad \text{Eq. 15}$$

Where  $f$  is the reference frequency (297.2 MHz), and  $\Delta f$  is -3 dB bandwidth [23]. VNA has an option to calculate the  $Q_{ratio}$  automatically. Therefore, it suffices to measure the tuning signal with pickup loops with and without the sample (Fig. 41).

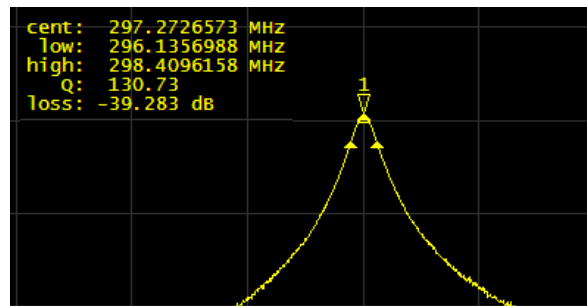


**Figure 41:  $Q_L$  calculated by VNA.**

Q-factor was measured for CH1 and CH5 in three different situations:

- Antenna + tuning and matching,
- Antenna + tuning and matching + active decoupling, and
- Antenna + tuning and matching + active decoupling + passive decoupling.

It has been experienced when the elements of the passive decoupling were added to the channels the  $Q_{ratio}$  was decreased. It means that significant amount of losses were induced in the circuitry and elements of the passive detuning. Consequently, passive detuning from all the channels has been removed. The remaining circuitry was isolated with Kapton® for all the channels.

### 3.3.1.5 Metal shield test

Metal shield test, which simulates the gradient coil, is a useful evaluation to study the influences of the metals on the receiver coil. For this test, CH1 and CH5 were isolated from each other by use of overlapping. Coupling levels between the channels were simultaneously monitored through  $S_{21}$ . Through Smith chart, the impedances and the changes of the channels were observed while the receiver coil was placed inside the transmitter coil and both of them were inserted within the metal shield (Fig. 42).

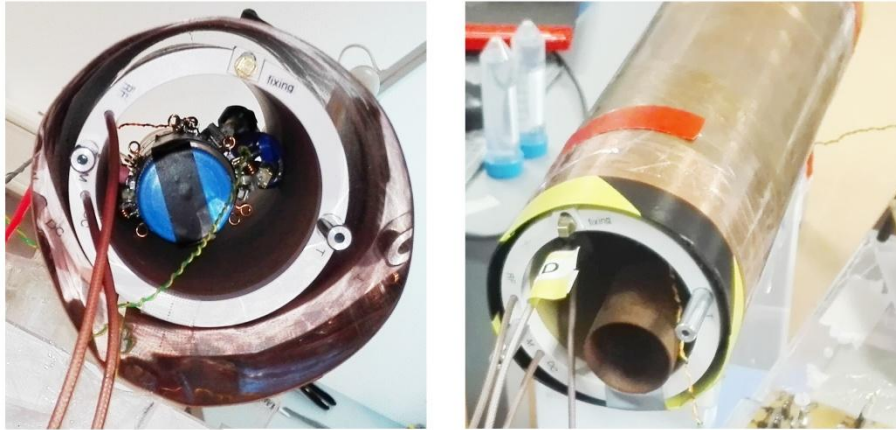


Figure 42: Setup of the metal shield test.

## 3.3.2 MR measurements

### 3.3.2.1 MR scanner

The performance of the coil in MR was evaluated in a 7T whole-body scanner (Magnetom 7T MRI, Siemens AG, Erlangen, Germany). The system is equipped with a SC72d gradient coil which presents a maximum gradient strength of 70 mT/m. However, for MRM investigations, these gradients must be switched off.

### 3.3.2.2 Micro-gradient system

Exclusively for MRM, a micro-gradient system should be mounted on the patient table to produce the strong gradients for microscopy. Electrically, the scanner must be switched to microscopy system. Therefore, the gradient system of the whole-body scanner is turned off and only the main field  $B_0$  of the scanner is being applied for the micro-gradient system. For microscopy purposes, a special computer must be also turned on while the computer of the whole-body scanner is shut down. Fig. 43 shows the micro-gradient system and its installation place.

Micro-gradient system has the following specifications [9]:



Manufacturer: Resonance Research, Inc., Billerica, MA, United States.

Maximum gradient strength: 750 mT/m.

Bore diameter: 92 mm.

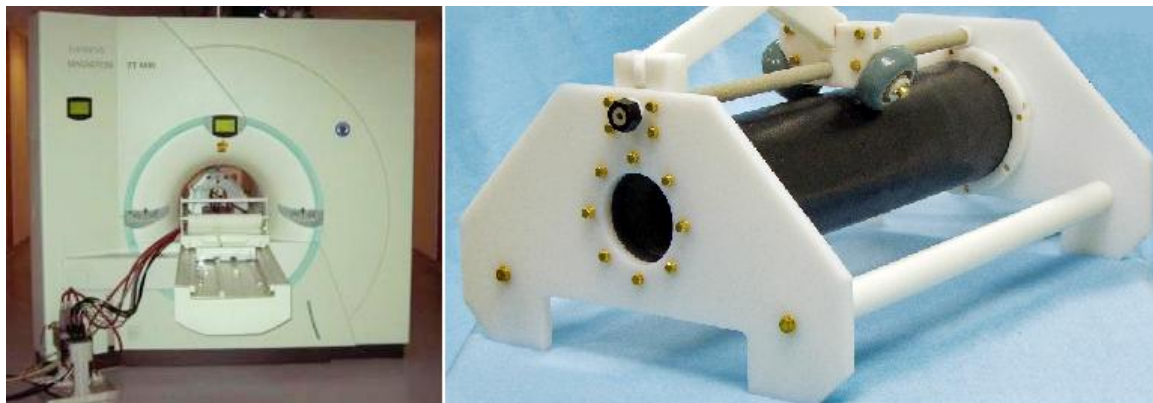


**Figure 43: Micro-gradient system and scanner installation.**

### **3.3.2.3 MR experiments**

The 8 channel receiver coil was placed and fixed inside the transceiver coil ( $^1\text{H}$  297 MHz, Rapid Biomedical, Rimpar, Germany). Through a dongle, the transceiver was set to operate as a transmit-only coil otherwise the combination of the 8 channel receive-only coil with the 72 mm transceiver did not make sense.

Three MR experiments were performed to evaluate the 8 channel receive-only coil. The feedback of the first measurement has been used to improve the hardware of the coil e.g. adding the wound coaxial cable traps.

#### *3.3.2.3.1 MR experiment 1: Homogeneous cylindrical saline phantom*

In order to evaluate the general function of the coil such as the performance of the every individual channel, effective FOV, and transmission decoupling, a standard sample container (Falcon<sup>™</sup> 50 mL conical centrifuge tube, L: 115 mm,  $\text{\O}$ : 30 mm) which was filled with  $\text{H}_2\text{O} + \text{NaCl}$  (0.45 S/m) was used. Imaging was processed by using gradient-recalled-echo (GRE) ( $\text{TR/TE} = 400 \text{ ms} / 3.5 \text{ ms}$ ) in two different views, coronal ( $\text{FOV: } 179 \times 411$ , Slice thickness: 5, Resolution matrix:  $56 \times 128$ ) and transversal ( $\text{FOV: } 150 \times 150$ , Slice thickness: 10, Resolution matrix:  $128 \times 128$ ).

### 3.3.2.3.2 MR experiment 2: Asparagus

For the second experiment, an asparagus was subjected to the scanner. A cross section cut from the front side of the asparagus was placed inside the sample container. The rest volume of the container was filled with tap water. For this experiment, a voxel size of about  $0.58 \times 0.58 \times 2 \text{ mm}^3$ , which is close to microscopy dimensions, was applied.

- Sequence information for sagittal imaging:  
Turbo spin-echo, TR/TE = 3000 ms / 8.2 ms  
FOV:  $140 \times 220$ , Resolution matrix:  $328 \times 512$ , Slice thickness: 2
- Sequence information for coronal imaging:  
Turbo spin-echo, TR/TE = 3680 ms / 7.7 ms  
FOV:  $148 \times 148$ , Resolution matrix:  $256 \times 256$ , Slice thickness: 2

### 3.3.2.3.3 MR experiment 3: Resolution phantom

In this measurement, evaluation of the coil for a resolution phantom (8 mmol/l, CuSO<sub>4</sub>), which is used for quality control, was performed. The sample is a special silicon wafer with periodically arranged slits between 64 and 2048  $\mu\text{m}$  [9]. Phantom was placed at the center of the receiver coil where the  $B_1^+$  center is also positioned. Turbo spin-echo (TR/TE = 1000 ms / 7.7 ms, FOV:  $120 \times 120$ ) sequence was applied for 55 seconds.

Furthermore, SNR for two different protocols were calculated. It has been suggested that to calculate the SNR, the mean signal of interest (center of the ROI) should be compared to the standard deviation of the signal of no interest (background of the image). Standard deviation of the background noise should be averaged from several regions [5].

- Sequence information to estimate the SNR (Image right):  
Turbo spin-echo, TR/TE = 136 ms / 4.1 ms  
FOV:  $100 \times 100$ , Resolution matrix:  $256 \times 256$ , Slice thickness: 15
- Sequence information to estimate the SNR (Image left):
- Turbo spin-echo, TR/TE = 136 ms / 4.1 ms
- FOV:  $100 \times 100$ , Resolution matrix:  $256 \times 256$ , Slice thickness: 1

# 4 Results

In MRI, testing and evaluation of the RF coils can be performed through simulation, bench measurement, and scanner test. Usually, simulation is considered for the transmitter or transceiver coils but there is no specific regulation for receive-only coils. Instead, bench and MR measurements must be done for all types of the coils.

## 4.1 Bench Measurement

Bench measurements can be easily performed during the development of the coil in the electronic lab. Results of the bench measurements can predict the performance of the coil in the scanner. It has been suggested that four coil characteristics namely tuning, transmission decoupling, mutual decoupling, and preamplifier decoupling should be optimized before evaluation of the coil in MR scanner [23]. Furthermore, estimating the resistive losses in the sample and the coil can be also performed by measuring the Q-factor.

### 4.1.1 Tuning and matching

At the final stage of the development, all the channels have been tuned and matched for the last time. Results are listed in table 7.

Results show that the channels were tuned at  $\omega_0 \pm 1$  MHz, which is an acceptable tolerance (for narrowband). Impedances were matched to  $75 \Omega$ . But some levels of reactance were always observed. This reactance before overlapping was too low but as soon as the arrays were being overlapped, this part of the impedance was increased.

**Table 7: S-parameters of tuning and matching**

	Channel	Tuning (MHz)	Impedance ( $\Omega$ )
Row 1	1	297.325	75 - j12
	2	297.137	75 - j8
	3	298.875	75 + j3
	4	298.012	75 - j26
Row 2	5	297.137	75 - j50
	6	297.200	75 - j45
	7	298.262	75 - j31
	8	297.887	75 - j40
	Average:	297.729	75 - j26

#### 4.1.2 Estimating the Q-factor

At the very beginning of the project,  $Q_{ratio}$  of the test prototype was measured to estimate the losses of the selected coil size and geometry. Additionally,  $Q_{ratio}$  of two different channels from different rows of the PCB were also calculated to find the source of the losses.

The results and steps are as follows:

- Test prototype:

$$Q_{ratio} = \frac{Q_U}{Q_L} \Rightarrow Q_{ratio} = \frac{120}{70} \Rightarrow Q_{ratio} = 1.7$$

- PCB elements: CH1 and CH5 without neighbor channels:

- Situation 1: Antenna + tuning and matching:

$$Q_{ratio} = \frac{170}{85} \Rightarrow Q_{ratio} = 2$$

- Situation 2: Antenna + tuning and matching + active detuning:

$$Q_{ratio} = \frac{130}{80} \Rightarrow Q_{ratio} = 1.6$$

- Situation 3: Antenna + tuning and matching + active detuning + passive detuning:

$$Q_{ratio} = \frac{74}{54} \Rightarrow Q_{ratio} = 1.3$$

Accordingly, adding more components to the channels results in more losses. It can be seen that the  $Q_{ratio}$  was significantly decreased by adding the diodes. Therefore, the components of the passive detuning were removed. Furthermore, it was observed that the signal was shifted to the right (ca. 300 kHz) during the measurement of the  $Q_U$ .

### 4.1.3 Influence of metal shield

As explained in section 3.3.1.5, the test was implemented for the CH1 and CH5 while the receiver coil was inside the transmitter coil and both were located within a metal shield. A comparison between results of the both channels showed that the impedance was changed about  $\pm 5 \Omega$ , but the coupling at the presence of metal shield was increased around 10 dB (from -28 dB to -18 dB). The changes in impedance due to the test were estimated negligible.

### 4.1.4 Transmission decoupling

Minimum level of isolation between tuning and detuning (receiver and transmitter mode) was measured about -40 dB. The dip of the signal was located at  $\omega_0 \pm 7$  MHz. The peaks were observed at  $\omega_0 + 102$  MHz and  $\omega_0 - 80$  MHz which shows about 10 MHz differences in order to be completely symmetrical.

### 4.1.5 Preamplicifier decoupling (PCB array)

Decoupling at  $\omega_0$  results in reduction of the mutual induction of the other channels. The dip of the signal must be at  $\omega_0$  and its difference from the horizontal axis defines the isolation level which can be obtained by the preamplifier. The test was performed individually for all the channels. Pickup loops through the  $S_{21}$  or  $S_{12}$  measured the decoupling signal when the preamplifier was plugged. The average level of decoupling of all the channels will be added to the level of mutual decoupling in the next section. It means more isolation of the channels and thus better performance of the coil. Table 8 shows the results of the preamplifier decoupling for each channel.

**Table 8: Decoupling levels caused by preamplifier**

	Channel	Decoupling (dB)
Row 1	1	-15
	2	-16
	3	-19
	4	-18
Row 2	5	-16
	6	-14
	7	-23
	8	-22
		<i>Average <math>\cong -18</math> dB</i>

#### 4.1.6 Mutual decoupling (test prototype, PCB array)

One of the important tests on the bench is the evaluation of isolation or mutual coupling. It influences signal quality because it causes splitting of the signal at  $\omega_0$ . Mutual coupling becomes more important when the channels are in an array and placed very close to each other. This is exactly the case in microscopy RF coils. Therefore, any effort to reduce the coupling is valuable. In order to implement the test, calibrated cables were connected to the output of the two different channels. During the test, all the other outputs were closed with a  $75 \Omega$  resistor. It means there was no preamplifier.  $S_{12}$  or  $S_{21}$  showed the decoupling levels on the VNA. This level had to be below from -10 dB. Reducing the coupling in an array was only possible with changing the small inductors between the channels. Although, decreasing the coupling between the arrays have been done by overlapping. Practically, each row consists of 4 channels was decoupled separately. The elements on the 1<sup>st</sup> row were decoupled from each other while the other elements on the 2<sup>nd</sup> row were located at distance and vice versa. After that, two channels of different rows, which faced each other, were connected to the VNA. The overlapping was started and being continued until the maximum decoupling level was obtained.

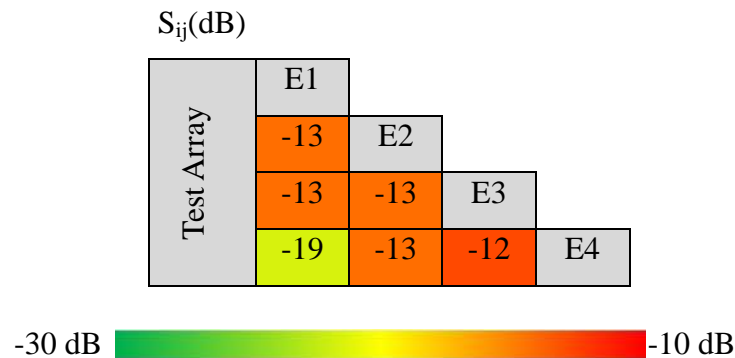
Since the method of transformer decoupling was very important to reduce the coupling between the opposing channels in an array, this test was also applied for the test prototype.

As mentioned before, the results of the  $S_{12}$  were written in an S-matrix. The results of the bench measurement are presented in this section.

#### 4.1.6.1 Mutual decoupling of test prototype

Performing this test was very critical to understand the function of the transformer decoupling for opposing channels. In this experiment, 4 single-test loops, which were placed around the tube, were constructed without transmission and preamplifier decoupling circuitries. Channels were only tuned at  $\omega_0$  and matched with transmission lines. Results showed that the range of isolation between opposing channels (E1, E3 and E2, E4) became similar to the adjacent elements by applying small inductors for opposing channels. Opposing channels without transformer decoupling presented a slightly split signal with the maximum isolation level of about -8 dB. With transformer decoupling the average isolation were increased to about -14.5 dB.

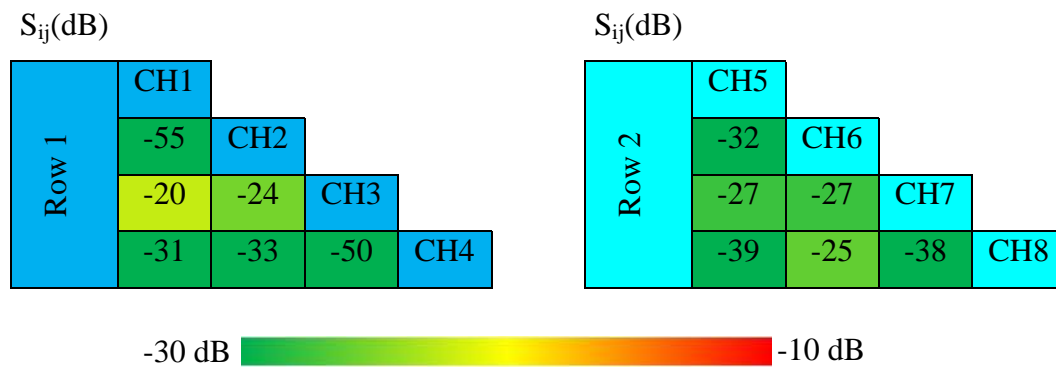
**Table 9: S-matrix of mutual coupling for array prototype**



#### 4.1.6.2 Mutual decoupling of separate rows on the PCB

It has been tried to get the maximum level of isolation between the channels in an array before overlapping. The method of transformer decoupling was applied not only between the adjacent elements but also for the elements which faced each other. The lowest isolation or maximum coupling (-20 dB) was observed between CH1 and CH3 which faced each other. However, this level of coupling was in a standard range. The averages of about -32 dB and -31 dB were measured for row 1 and row 2, respectively.

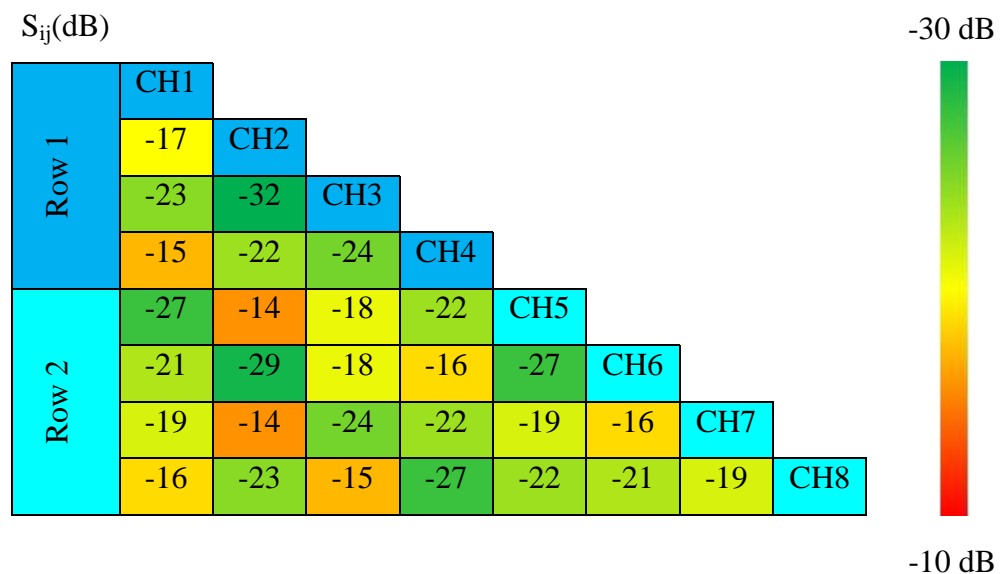
**Table 10: S-matrix of mutual coupling for non-overlapped arrays**



#### 4.1.6.3 Mutual decoupling of the 8 channel receive-only coil (with floating cable traps)

In this test, arrays were overlapped and only one floating cable trap was used for the scanner cable to reduce the common mode. The average isolation of the rows was reduced to -20 dB, which was about 35% decreasing. The highest coupling was measured from the channels which located in different rows and facing each other, e.g. CH2 and CH7 with -14 dB. However, a level of -15 dB was also observed for adjacent channels like CH1 and CH4. Finally, total decoupling levels ranged from -14 dB to -32 dB with a mean value of about -20 dB. This level of isolation was very good and it was improved with an additional average isolation level of the preamplifier decoupling which was about -18 dB.

**Table 11: S-matrix of mutual coupling for 8 channel receive-only coil**

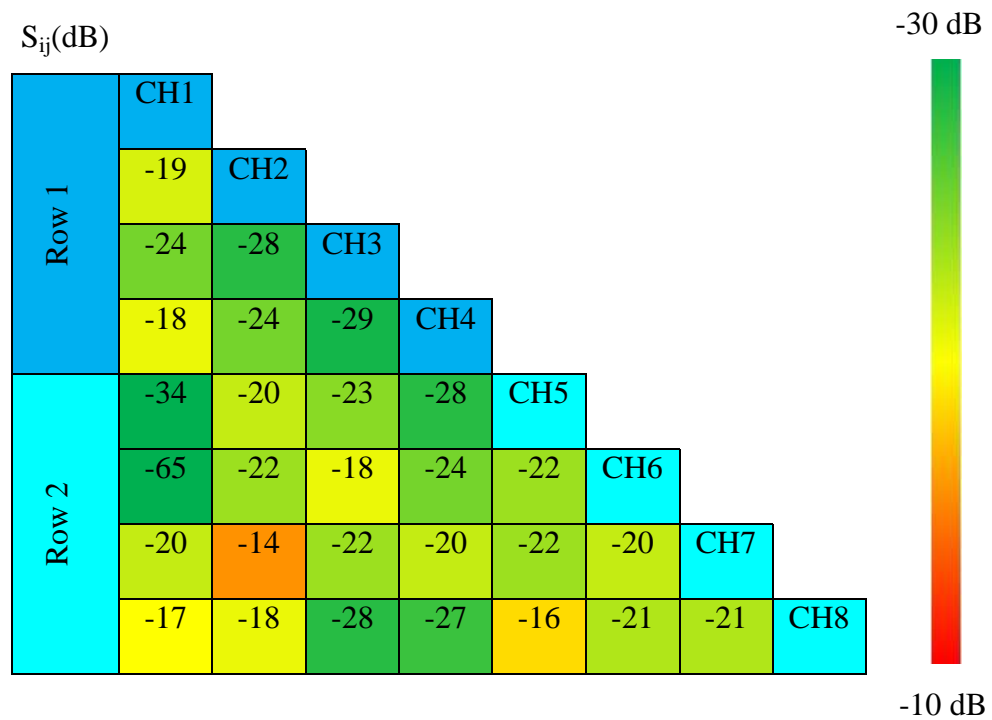




#### 4.1.6.4 Mutual decoupling of the 8 channel receive-only coil (with wound coaxial and floating cable traps)

After analyzing the results of the first imaging, wound coaxial cable traps were built and connected to the each channel of the coil. Every cable trap has been carefully constructed to resonate at  $\omega_0$  and connected to the signal cables after preamplifiers. Results of the bench were improved in comparison with the last situation which had only a floating cable trap. Isolation between most of the channels looks more homogeneous. However, the average level of isolation was improved about 7%. An average level of about -21.5 dB was obtained for the whole elements. With this technique, the image quality, which had been degraded in previous section, was also enhanced.

**Table 12: Improved results of mutual coupling for 8 channel receive-only coil**



## 4.2. MR Measurements

### 4.2.1. Experiment 1: Homogeneous cylindrical saline phantom

Fig. 44 shows the 8 coronal slices of the sample from 8 different channels. As it was predicted after overlapping, a complete coverage of the sample was obtained. The length of the sample is about 115 mm, which is covered by the 8 channel receive-only coil.

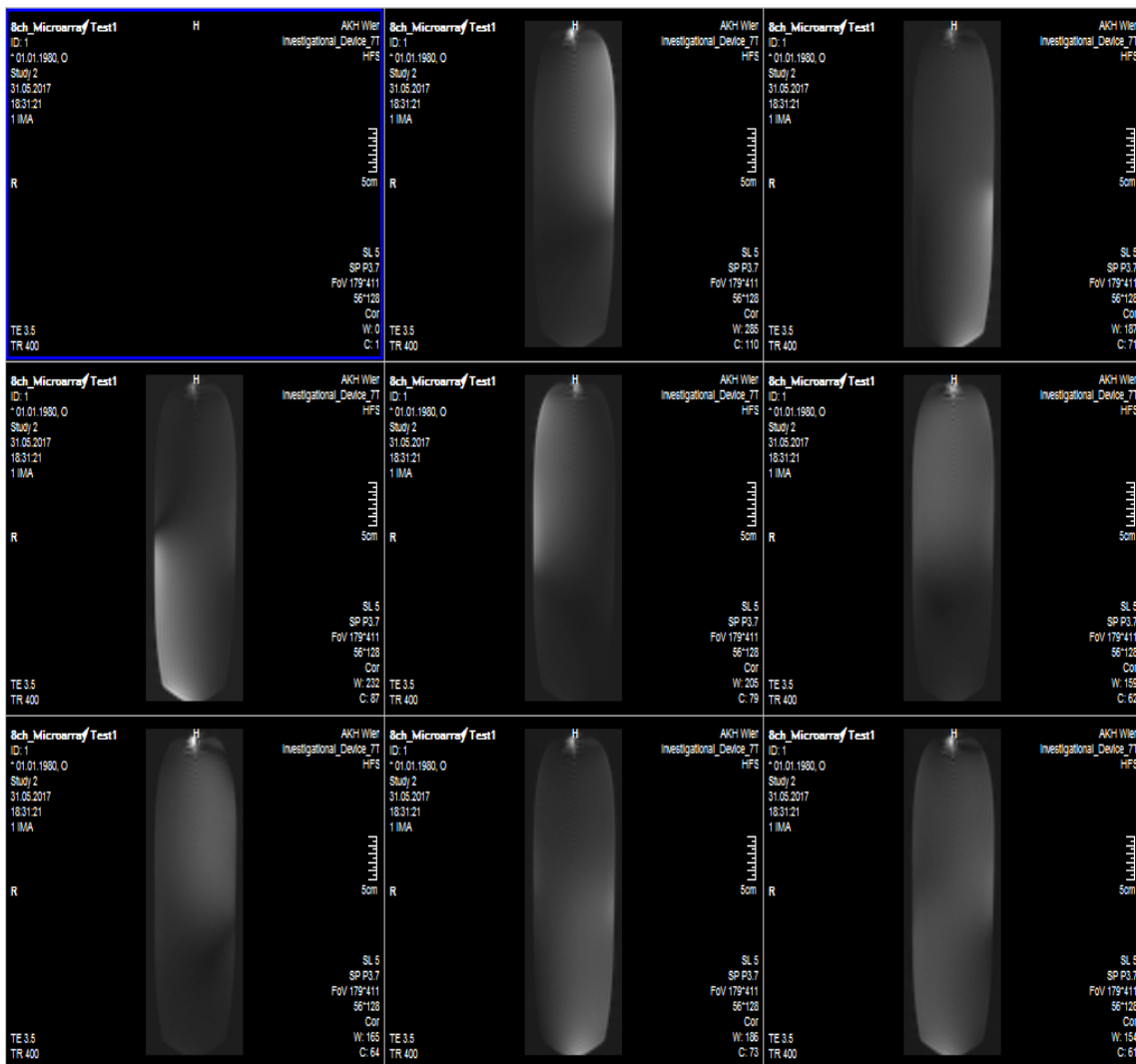
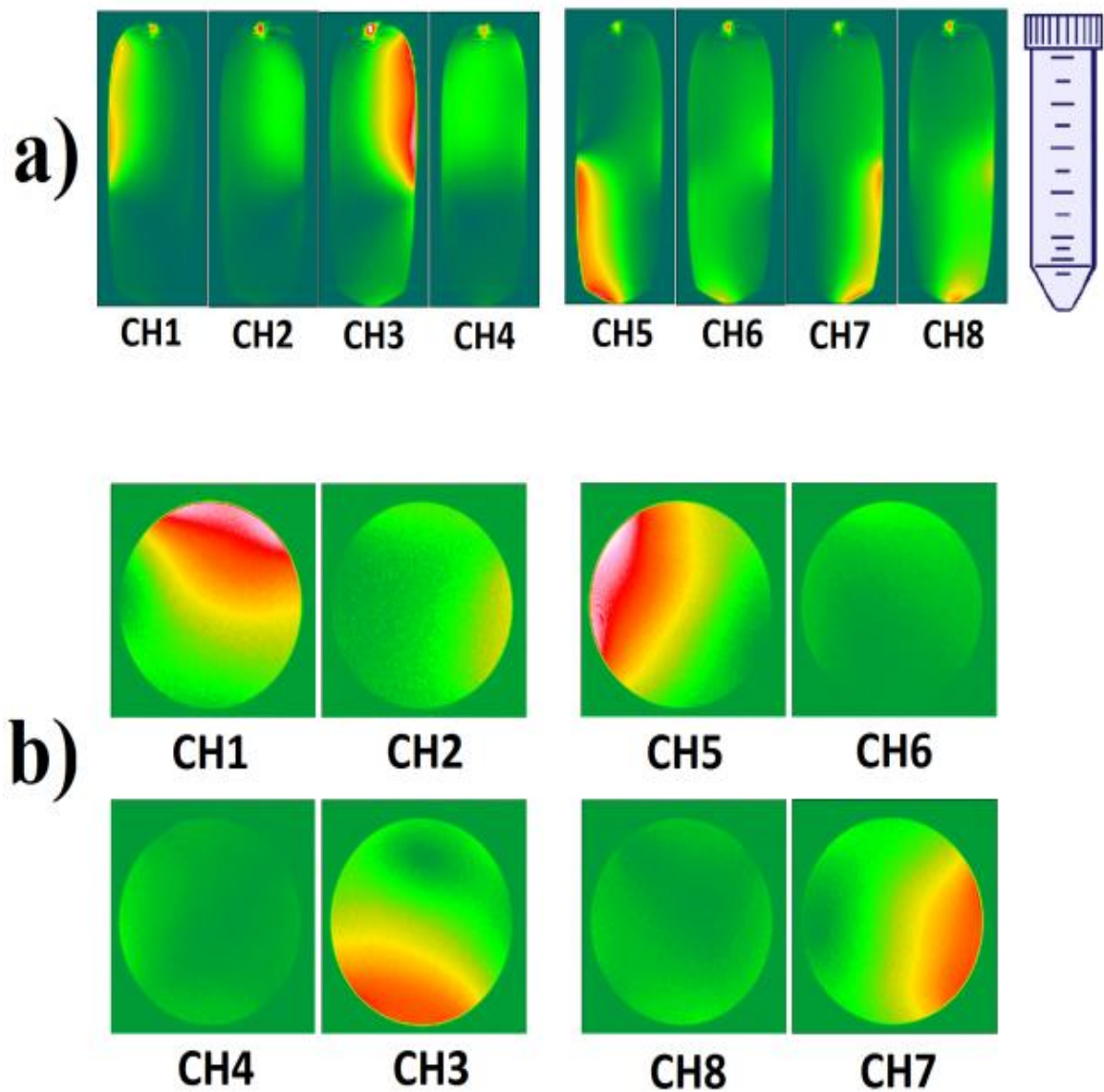


Figure 44: First imaging result of 8 channel receiver coil.

Furthermore, coronal and transversal slices were manipulated to evaluate the homogeneity of the coil (Fig. 45). It was observed that some channels apparently operate stronger than the others which cause inhomogeneity in the whole FOV. This inhomogeneity was enhanced for the second imaging experiment.



**Figure 45: Evaluating the homogeneity. a) Coronal view. b) Axial view.**

### 4.2.2. Experiment 2: Asparagus

In this experiment, the tissue coverage and the performance of the coil at microscopy levels were successfully evaluated. Fig. 46 shows the visible anatomy of the asparagus in different sections (coronal and axial). The smallest visible structure was calculated about 0.1 mm.

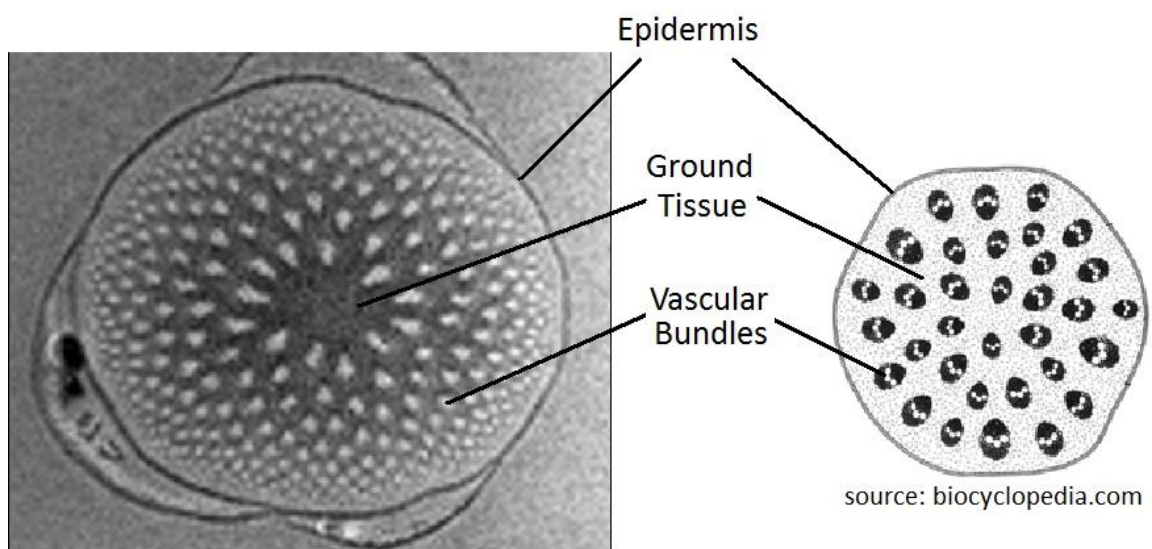
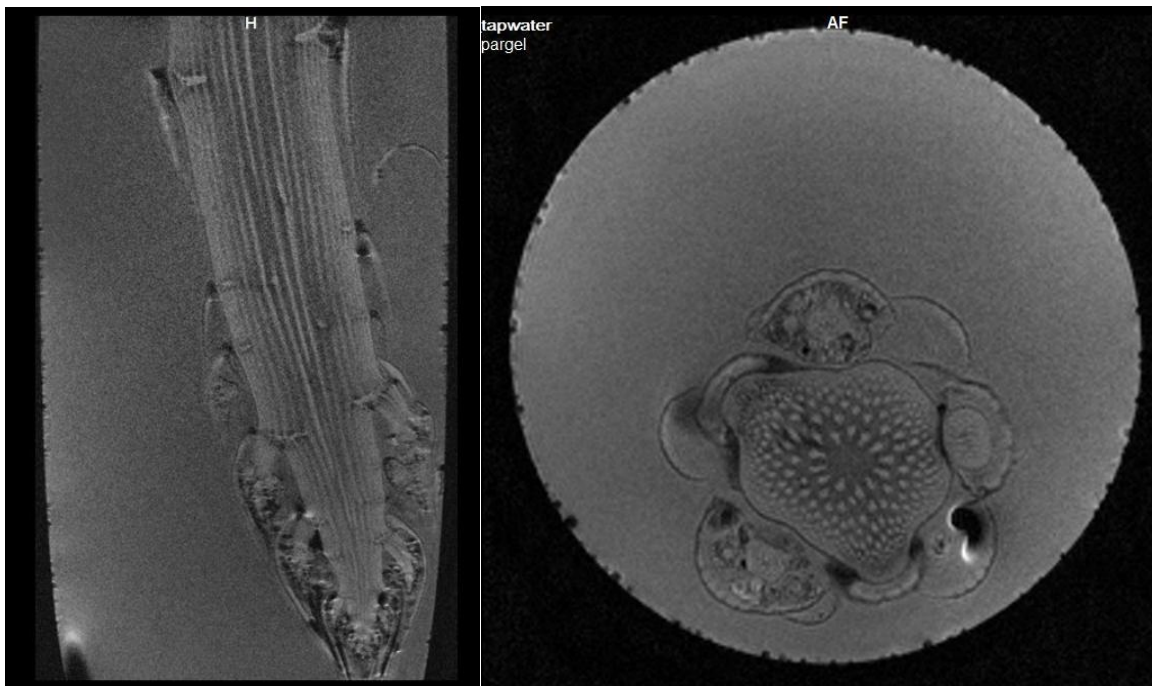


**Figure 46: MR imaging of asparagus.**

### 4.2.3. Experiment 3: Resolution phantom

In comparison with the first experiment, a better  $B_1^+$  homogeneity was observed (Fig. 47a). Resolution of about 0.097 mm was observed on the resolution phantom (Fig. 47b).

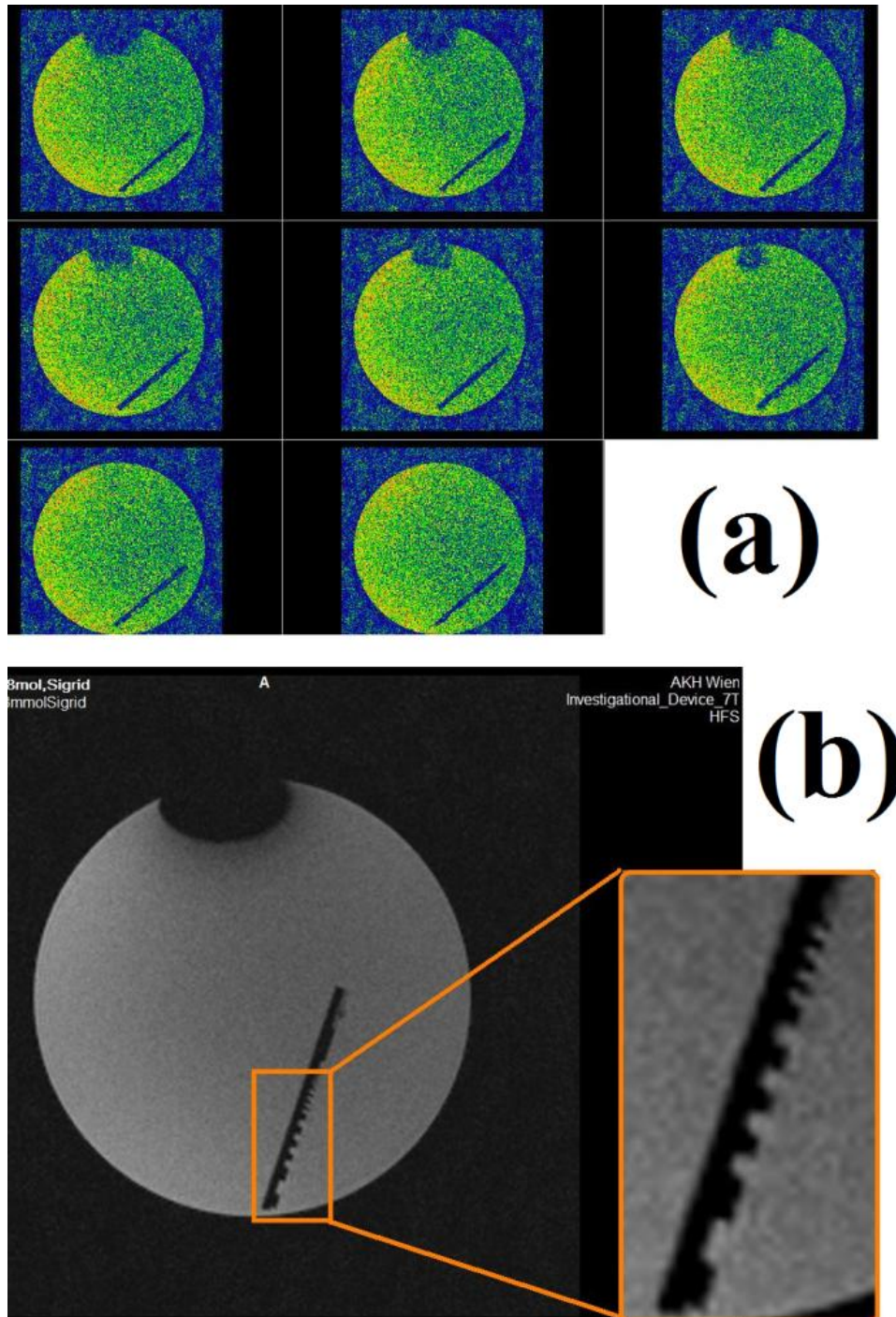


**Figure 47: MR imaging on resolution phantom.**  
a) Axial of the phantom. b) Estimating the resolution.



Fig. 48 shows two different images which have been obtained with two different protocols. Higher SNR in the right image was achieved when the slice thickness increases from 1 to 15 which is one of the issues listed in Table 2.

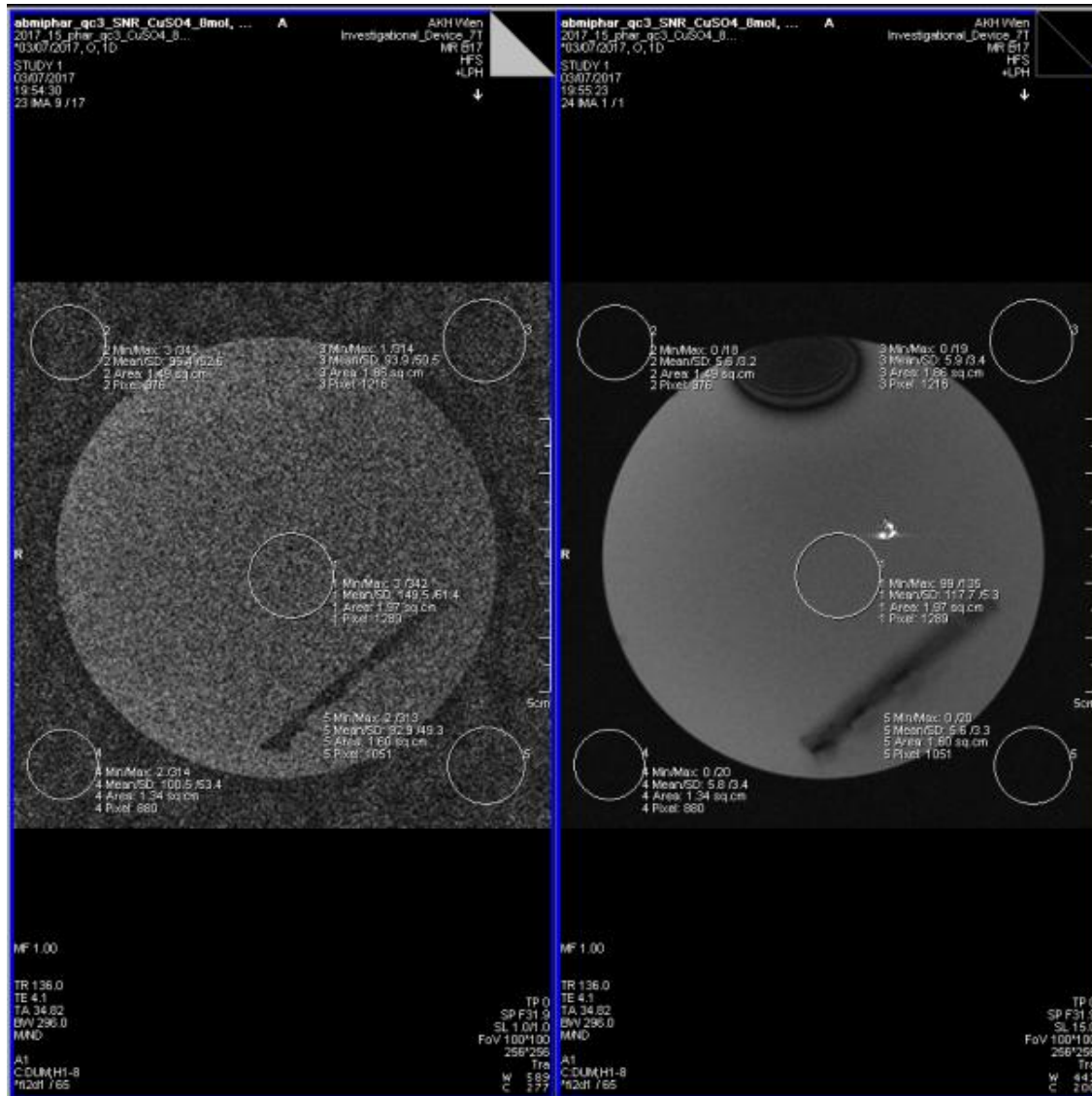


**Figure 48: SNR comparison. Left image = 1.57, right image = 20.43.**

#### 4.2.4. Experiment 4: Parallel imaging performance

Fig. 49 demonstrates the 12 different images which were processed in Matlab. It can be observed that the more accelerated imaging results in a less SNR. Accordingly, when  $R = 2$ , the SNR is acceptable and there is no aliasing. For faster imaging times,  $R > 2$ , SNR will be significantly decreased. It can be seen when  $R = 4$ , signal intensity at the center of the phantom is similar to the background which means less SNR.

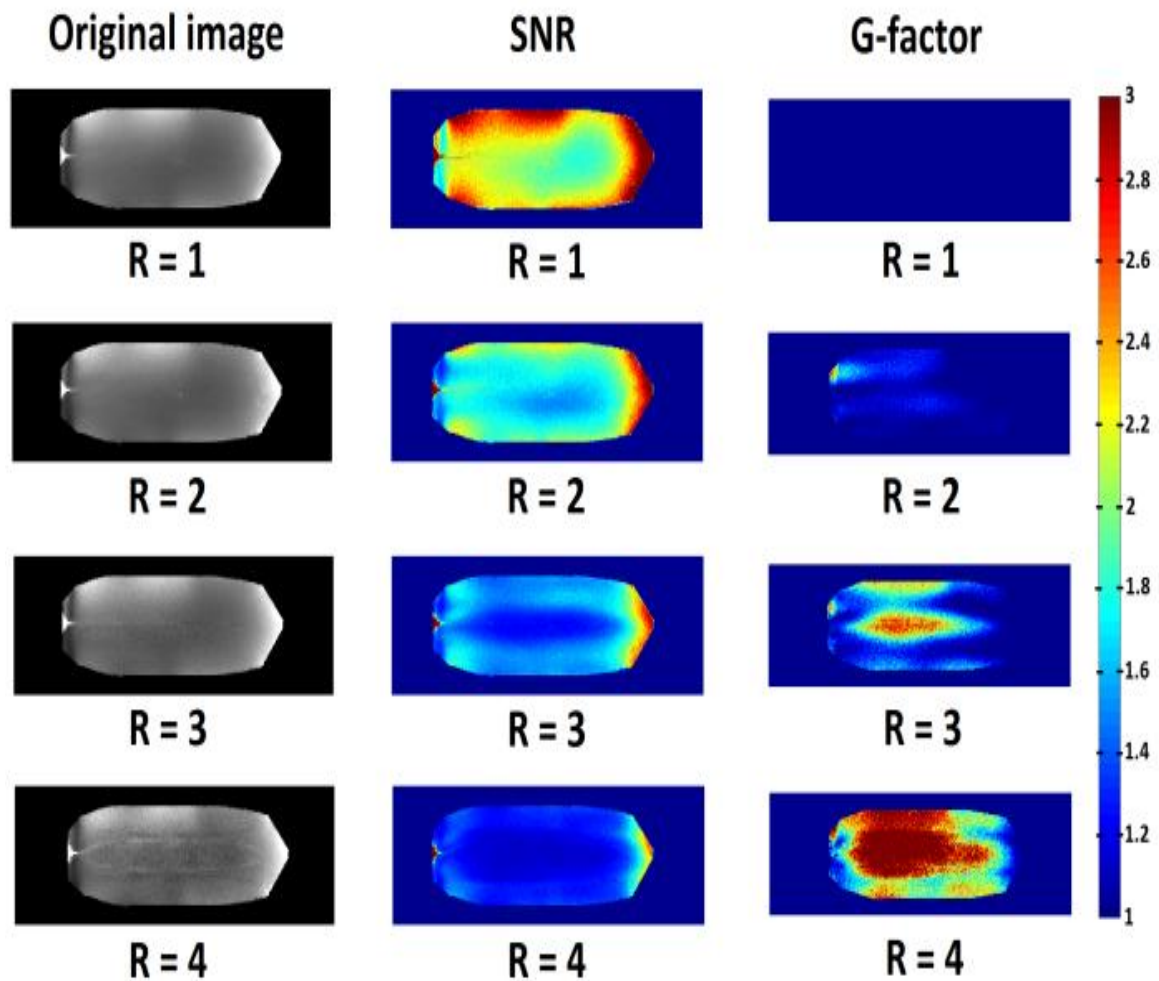


Figure 49: G-factor vs. SNR.





# 5. Discussion and Outlook

## 5.1. Discussion

In this project, a tube-shaped 8 channel receive-only coil array for MRM at 7T was developed. The inner and outer sizes of the coil were limited by an available commercial transmitter ( $^1\text{H}$  297 MHz, Rapid Biomedical, Rimpar, Germany) and also by different sample containers which used for various applications. Therefore, the main challenge of the project was to implement the coil in a small space. For this reason, selecting the proper components to meet the requirements became very important. On the other hand, in order to accelerating the imaging time, the number of receiver channels added more barriers to the project.

In this work, the antenna elements and their circuitries were designed on a flexible PCB which resulted in saving more space and to have an equal form and size for all the 8 channels. Instead, due to the material sensitivity of the PCB, a more protectively work was expected. In particular, solder pads had been attached to the PCB through an adhesive material which had a thickness of about 0.025 mm. Since the adhesive was sensitive to temperature, solder wires with a lower melting point have been used. Furthermore, some special soldering Tips as well as cleaning agents like flux were applied to remove the oxidations. Although, the abovementioned issues have been considered, a few solder pads were detached. Trial and error has an important role during the coil manufacturing. Therefore, soldering and desoldering a component can be repeated many times in order to find the proper value of the element. As a result, the material of the PCB should be enough stable during the manufacturing process.

Regarding SNR and accelerating factors, some issues should be considered. SNR depends not only on the sensitivity of the RF coil but also on the parameter settings of the imaging protocol. Hence, to evaluate the SNR of the receiver coil, a comparative study should be performed. For instance, to compare the SNR between two different coils, a same protocol and a same sample must be applied.

In order to increase the MR signal, low noise preamplifiers with  $75\ \Omega$  input impedance were placed as close as possible to the channels. Ideally, to adjust the impedance of the receiver channels to  $75\ \Omega$ , impedance of the cables, connectors and the input of the VNA

should be also 75  $\Omega$ . However, this was not achievable in this project because the standard impedance of the most electronic devices is 50  $\Omega$ .

Despite technical challenges, using low noise preamplifiers and methods of mutual decoupling could increase the isolation between the channels and thus improved the MR signal.

## **5.2. Conclusions and suggestions for further work**

This thesis presented a highly sensitive 8 channel receive-only coil array for MRM at 7T which is successfully developed to be used for microscopy investigations. In order to have a miniature design and precise coil geometry, receiver channels implemented on a flexible printed circuit board. Performance of the coil was validated with bench and imaging measurements. A very good homogeneity over a large FOV was achieved with different samples. Construction of the array has potential for applying parallel imaging with a reasonable SNR.

For further studies, different pulse sequences can be experienced with the receiver coil to find a proper protocol which can improve the efficiency of the coil. In order to select a proper coil for a specific application, comparative investigations can be done between the receiver coil and other available coils. By adding fuses to the channels and increasing the safety of the coil, the receiver can be applied for in vivo examinations.

# 6. Appendix

## 6.1. Bibliography

- [1] Gimi, Barjor. *"Magnetic resonance microscopy: concepts, challenges, and state-of-the-art."* Magnetic Resonance Imaging: Methods and Biologic Applications (2006): 59-84.
- [2] Prasad, Pottumarthi V., ed. *Magnetic resonance imaging: methods and biologic applications*. Vol. 124. Springer Science & Business Media, 2006.
- [3] Kuperman, Vadim. *Magnetic resonance imaging: physical principles and applications*. Academic Press, 2000.
- [4] Suetens, Paul. *Fundamentals of medical imaging*. Cambridge university press, 2009.
- [5] Lipton, Michael L. *Totally accessible MRI: a user's guide to principles, technology, and applications*. Springer Science & Business Media, 2010.
- [6] Hennig, Jürgen, and Oliver Speck. *High-field MR imaging*. Springer, 2012.
- [7] Moser, Ewald, et al. *"7-T MR—from research to clinical applications?."* NMR in Biomedicine 25.5 (2012): 695-716.
- [8] Kraff, Oliver, et al. *"MRI at 7 Tesla and above: demonstrated and potential capabilities."* Journal of Magnetic Resonance Imaging 41.1 (2015): 13-33.
- [9] Berg, A., A. Potthast, and P. Starewicz. *"MR-Microscopy on a Human 7T Scanner."* Proc. Intl. Soc. Mag. Reson. Med. Vol. 18. 2010.
- [10] Doty, F. David, et al. *"Radio frequency coil technology for small-animal MRI."* NMR in Biomedicine 20.3 (2007): 304-325.
- [11] Mispelter, Jo, Mihaela Lupu, and Andr Briguet. *NMR probeheads for biophysical and biomedical experiments: theoretical principles & practical guidelines*. Imperial College Press, 2006.
- [12] Weishaupt, Dominik, Victor D. Köchli, and Borut Marincek. *How does MRI work?: an introduction to the physics and function of magnetic resonance imaging*. Springer Science & Business Media, 2008.
- [13] Wikipedia contributors. *"Antenna (radio)."* Wikipedia, The Free Encyclopedia. Wikipedia, The Free Encyclopedia, 30 Jul. 2017. Web. 31 Jul. 2017
- [14] Hui, Hon Tat. *"Decoupling methods for the mutual coupling effect in antenna arrays:"*

- A review.*" Recent Patents on Engineering 1.2 (2007): 187-193.
- [15] Avdievich, N. I., and H. P. Hetherington. "*4T Actively detuneable double-tuned 1 H/31 P head volume coil and four-channel 31 P phased array for human brain spectroscopy.*" *Journal of Magnetic Resonance* 186.2 (2007): 341-346.
- [16] Haase, Axel, et al. "*NMR probeheads for in vivo applications.*" *Concepts in Magnetic Resonance Part A* 12.6 (2000): 361-388.
- [17] Reykowski, Arne, Steven M. Wright, and Jay R. Porter. "*Design of matching networks for low noise preamplifiers.*" *Magnetic resonance in medicine* 33.6 (1995): 848-852.
- [18] Elster AD. <http://mriquestions.com/index.html>
- [19] Deshmane, Anagha, et al. "*Parallel MR imaging.*" *Journal of Magnetic Resonance Imaging* 36.1 (2012): 55-72.
- [20] Application note. *Understanding the Fundamental Principles of Vector Network Analysis*: Agilent Technologies, Inc. 2012, Published in USA, December 12, 2012, 5965-7707E.
- [21] Keeler, James. "*Understanding NMR Spectroscopy (2004).*" (2016).
- [22] Darrasse, Luc, and Ghazi Kassab. "*Quick measurement of NMR-coil sensitivity with a dual-loop probe.*" *Review of scientific instruments* 64.7 (1993): 1841-1844.
- [23] Keil, Boris, et al. "*A 20-channel receive-only mouse array coil for a 3 T clinical MRI system.*" *Magnetic resonance in medicine* 66.2 (2011): 582-593.
- [24] Keil, Boris. "*Construction of Receive Arrays.*"
- [25] Eberler, Ludwig, Wolfgang Renz, and Guenther Zebelein. "*Dividing wall separating the RF antenna from the patient chamber in an MR scanner.*" U.S. Patent No. 7,501,826. 10 Mar. 2009.
- [26] Janezic, Michael D., N. G. Paulter, and J. E. Blendell. "*Dielectric and conductor-loss characterization and measurements on electronic packaging materials.*" *NIST Technical note* 1520 (2001).
- [27] Datasheet. <http://www.pcb-pool.com>.
- [28] Giaquinto, R.O., Piel, J.E. *Coil Performance vs. Preamplifier Location in the MR Phased Array*. GE Global Research Center, Niskayuna, New York, United States. 2009.
- [29] Seeber, D. A., J. Jevtic, and A. Menon. "*Floating shield current suppression trap.*" *Concepts in Magnetic Resonance Part B: Magnetic Resonance Engineering* 21.1 (2004): 26-31.

## 6.2. List of Figures

Figure 1: Basics of magnetic resonance imaging .....	16
Figure 2: Dependency of the magnetic field to the position .....	18
Figure 3: Free induction decay .....	21
Figure 4: Different types of coils .....	22
Figure 5: Equivalent electrical circuit of a receiver coil.....	23
Figure 6: A simple receiver coil with tuning and matching elements.....	23
Figure 7: Function of the matching network.....	24
Figure 8: Tuning and detuning in receive and transmit modes.....	24
Figure 9: Voltage-current characteristic of one diode.....	25
Figure 10: Voltage-current characteristic of two diodes in passive decoupling .....	26
Figure 11: Circuit diagram of the active decoupling .....	26
Figure 12: Field of view by different coils .....	27
Figure 13: Effect of overlapping on mutual coupling.....	28
Figure 14: Concept of preamplifier decoupling.....	29
Figure 15: Sensitivity vs. depth for circular surface coils .....	32
Figure 16: Principles of scattering parameters.....	35
Figure 17: Smith chart .....	36
Figure 18: Birdcage transmit coil .....	40
Figure 19: Available sample containers .....	41
Figure 20: Single-test loop.....	44
Figure 21: Different coil configurations .....	45
Figure 22: Transformer decoupling between adjacent coils .....	46
Figure 23: Tuning and matching signals of four test loops in an array.....	47
Figure 24: Overlapping of two test loops. ....	47
Figure 25: Decoupled signal by preamplifier .....	48
Figure 26: Matching impedance at $75 \Omega$ .....	48
Figure 27: Possibilities of the matching network .....	49
Figure 28: Different circuit diagrams of transmission decoupling .....	51
Figure 29: Estimating the size and the shape of the coil.....	53
Figure 30: Components of the coil housing .....	54
Figure 31: Structure of the two layer flexible PCB .....	56
Figure 32: Schematic circuit diagram of a single channel.....	57

Figure 33: Schematic of the PCB of the receiver coil .....	60
Figure 34: Flexible PCB arrays.....	61
Figure 35: Channel isolation only by preamplifier decoupling .....	63
Figure 36: Removing the solder pad from the PCB.....	63
Figure 37: Final location of the arrays after overlapping .....	64
Figure 38: Different parts of the final receiver coil .....	67
Figure 39: Complete view of the 8 channel receive-only coil .....	68
Figure 40: Front side and back side views of transmit and receive coils .....	69
Figure 41: $Q_L$ calculated by VNA.....	71
Figure 42: Setup of the metal shield test.....	72
Figure 43: Micro-gradient system and scanner installation.....	73
Figure 44: First imaging result of 8 channel receiver coil .....	82
Figure 45: Evaluating the homogeneity .....	83
Figure 46: MR imaging of asparagus.....	84
Figure 47: MR imaging on resolution phantom.....	85
Figure 48: SNR comparison.....	86
Figure 49: G-factor vs. SNR .....	87

### 6.3. List of Tables

Table 1: Important magnetic resonance properties of useful nuclei .....	19
Table 2: Parameters to improve the SNR.....	33
Table 3: Useful devices and measuring tools.....	37
Table 4: Requirements and limitations of the coil housing.....	52
Table 5: Specifications of the flexible PCB .....	58
Table 6: List of the applied elements for the 8 channel receiver coil .....	65
Table 7: S-parameters of tuning and matching .....	76
Table 8: Decoupling levels caused by preamplifier .....	78
Table 9: S-matrix of mutual coupling in array prototype.....	79
Table 10: S-matrix of mutual coupling for non-overlapped arrays.....	80
Table 11: S-matrix of mutual coupling for 8 channel receive-only coil .....	80
Table 12: Improved results of mutual coupling for 8 channel receive-only coil .....	81

## 6.4. Publication List

- Hosseini E. et al. “8-channel receive-only coil array for MR microscopy at 7T”, abstract accepted in ESMRMB 2017, Barcelona, Spain.

## 6.5. Curriculum Vitae

### Education

- **Master of Biomedical Engineering** **03.2011 – 08.2017**  
*Vienna University of Technology*  
**Major:** Medical Physics & Imaging  
**Master thesis:** „Develop a highly sensitive 8 channel receive-only radio frequency coil array for microscopic magnetic resonance imaging at 7 Tesla”.
- **Bachelor of Science in** **09.2000 – 01.2005**  
**Electrical & Electronics Engineering**  
*Department of Electrical Engineering, Azad University of Sabzevar, Iran*  
**Bachelor thesis:** “PLC based automatic car parking system”.

### Work Experience

- **Medical University of Vienna, Austria** **09.2016 – Present**  
*Division MR Physics - Center for Medical Physics & Biomedical Engineering*  
**Position:** Research Intern
- **iSYS Medizintechnik GmbH, Austria** **02.2012 – 04.2016**  
*Manufacturer of Robotic Systems for Interventional Radiology*  
**Position:** Technical Employee (part time, 20 hours/week)